

State-Space Constraints Improve the Generalization of the Differentiable Neural Computer in some Algorithmic Tasks

Patrick Ofner, *Member, IEEE*, and Roman Kern

Abstract—Memory-augmented neural networks (MANNs) can solve algorithmic tasks like sorting. However, they often do not generalize to lengths of input sequences not seen in the training phase. Therefore, we introduce two approaches constraining the state-space of the network controller to improve the generalization to out-of-distribution-sized input sequences: state compression and state regularization. We show that both approaches can improve the generalization capability of a particular type of MANN, the differentiable neural computer (DNC), and compare our approaches to a stateful and a stateless controller on a set of algorithmic tasks. Furthermore, we show that especially the combination of both approaches can enable a pre-trained DNC to be extended post hoc with a larger memory. Thus, our introduced approaches allow to train a DNC using shorter input sequences and thus save computational resources. Moreover, we observed that the capability for generalization is often accompanied by loop structures in the state-space, which could correspond to looping constructs in algorithms.

Index Terms—differentiable neural computer, memory-augmented neural network, generalization, state-space, algorithmic tasks

I. INTRODUCTION

End-to-end learning and solving algorithmic problems with artificial neural networks (ANNs) has become a focus of research in recent years. Algorithmic problems were initially thought to be the domain of symbolic information processing. However, also the connectionism of ANNs is suitable for some algorithmic problems. For example, long short-term memory (LSTM) [1] and its variants can evaluate simple programs, add numbers, or memorize sequences of digits [2], [3]. Impressively, also question answering from short stories, London Underground route finding (i.e. graph traversal), or mastering a block puzzle game has been demonstrated with ANNs [4].

Although vanilla recurrent neural networks (RNNs) can theoretically already solve any algorithmic task as they are Turing complete [5], they are not sample-efficient enough to learn algorithmic tasks end-to-end in practice. Hence, several ideas emerged to enable ANNs to learn these tasks. One main idea is to augment an ANN with an external memory yielding a so-called memory augmented neural network (MANN). An MANN comprises an ANN-based controller and a memory

matrix. The controller learns to (1) compute the output based on the input and the memory content, and to (2) read and write the memory matrix via attention mechanisms [6]. The controller could be any ANN (e.g. feed-forward ANN or LSTM), and the MANN as a whole is an instance of an RNN. The Neural Turing Machine (NTM) [7] or its successor, the Differentiable Neural Computer (DNC) from Graves et al. [4], are two prominent representatives of this approach that can solve algorithmic tasks. Another neural network architecture that also features a directly accessible external memory is the so-called memory network [8]. However, memory networks were mainly tested and used in question and answering tasks or language modeling tasks rather than algorithmic tasks. Besides the aforementioned architectures featuring random memory access, more restricted memory access schemes based on stack architectures were developed [9]. An overview and a taxonomy of various RNNs with respect to their memory structure can be found in [10].

In parallel to the idea of augmenting ANNs with an external memory so that algorithmic tasks can be solved, other interesting approaches have been proposed. Pointer networks use attention for a pointer to select input symbols for the output [11]. The output values are direct references to the symbols rather than approximations calculated by the ANN. This makes pointer networks particularly suitable for algorithmic problems where output symbols correspond to input symbols. Also, convolutional connections were applied to algorithmic task learning. The Neural GPU uses convolutional gated recurrent units applied to the whole input sequence at once to learn algorithmic tasks [12]. Moreover, the Multigrid Neural Memory, a network architecture with a multigrid structure with distributed memory cells, has been proposed [13]. Contrary to the Neural GPU, this network is applied recurrently on the input sequence. The network is hierarchically organized with differently sized memory cells in each layer connected via convolutional operations. This way, the Multigrid Neural Memory network allows for data-dependent routing of information along short network routes. Another approach to learn algorithmic and other tasks was introduced by Goyal et al. [14]. The authors introduced a network architecture with multiple recurrent modules that interact only sparsely through an attention bottleneck, resembling dynamical processes in physical systems. Besides these approaches, also program synthesis has been researched. There, a program is often assembled from predefined primitive processing units, e.g. arithmetic or comparison operations (see [15]–[18] for exam-

P. Ofner was with the Area Knowledge Discovery, Know-Center GmbH, Graz, Austria. He is currently with the Bernstein Center Freiburg, University of Freiburg, Freiburg, Germany (e-mail: patrick@ofner.science).

R. Kern is with the Area Knowledge Discovery, Know-Center GmbH, and Graz University of Technology, Graz, Austria (e-mail: r.kern@know-center.at).

ple). However, program synthesis often requires supervision with execution traces impeding end-to-end learning, and/or is challenging for gradient descent-based optimization methods.

An important performance aspect of ANNs solving algorithmic tasks is how well they generalize to out-of-distribution samples. That is the performance on a test set that differs from the training set. For algorithmic tasks, these differences can be, for example, in the dictionary of the input symbols or the length of the input sequences. Especially, the latter is highly relevant in practice with MANNs like the DNC. With MANNs, training time increases with the sequence length of the input, and input length generalization would allow to train MANNs on short sequences and apply them afterward on longer sequences. Besides this practical aspect, the knowledge of how to facilitate input length generalization could offer valuable insights into how connectionist models process data.

Unfortunately, MANN-based architectures like NTM or DNC show only limited input length generalization. While there exists scientific work on performance improvements in general (e.g. [19]–[23]), work on improving particularly the input length generalization of the NTM or DNC is sparse. Le et al. [24] suggested loading controller weights dynamically via attention mechanisms from memory instead of using learned but otherwise fixed weights. That improved the input-length generalization performance in comparison to the NTM on, e.g. copy tasks. In [25], this work was extended by allowing the controller weights to represent shareable and modular programs. Yang et al. [26] utilized group theory and formalized memory access as group actions. They showed that a differentiable group (Lie group) allows input-length generalization to two-times longer input sequences than seen during the training phase for, e.g. sort or copy tasks. In addition, it was shown that sparse memory access could be beneficial for generalization [19].

In this work, we introduce approaches to improve the input length generalization capabilities of the DNC for some algorithmic tasks. We speculate that the input length generalization is limited because the controller state drifts eventually off into state-space regimes not seen in the training phase, which could lead to an unexpected controller behavior. As a remedy, we propose to promote loops in the state-space of the controller network and thus prevent the states from drifting into untrained regimes. From another point of view, state-space loops could also resemble the control flow of an algorithm that cycles over a limited set of possible instructions (e.g. loops over switch statements). In this view, state-space loops could facilitate learning of some algorithms as they provide an inductive bias towards such control flow structures. In particular, algorithms processing a variable number of input symbols in a row can often be realized with loops. To promote loops, we concretely suggest to (1) compress the state-space of the DNC’s controller, and alternatively, to (2) regularize the state-space so that new controller states are close to any already visited state. Compression is realized via an architectural adaption, whereas regularization is implemented by an additional term in the loss-function. Both approaches constrain the state-space and should introduce an inductive bias towards compacter state-spaces facilitating the emergence of state-space loops.

We test the approaches on algorithmic tasks with input-sequence lengths unseen during the training phase, and visualize the state-space of the DNC controller to reveal potential loop-like structures. Furthermore, we analyzed whether our approaches are compatible with extending a pre-trained DNC with a larger memory to process longer sequences.

II. BACKGROUND

We provide here the background of a particular instance of an MANN, namely the DNC [4], on which we tested our compression and regularization approaches. The DNC is an RNN and comprises a controller and a dedicated memory matrix which the controller accesses via attention mechanisms.

a) *DNC Memory*: The memory \mathbf{M} is organized as an $N \times W$ matrix, where the N rows are the memory slots, and the W columns correspond to the width of the memory slots. An attention mechanism calculates a weighting over all N memory slots, which is then used for writing or reading. The information read from memory is stored in a read vector $\mathbf{r}_t \in \mathbb{R}^W$ obtained as

$$\mathbf{r}_t = \mathbf{M}_t^\top \mathbf{w}_t^r$$

where t is the time index, and $\mathbf{w}_t^r \in \mathbb{R}^N$ is the read weighting vector. Analogously, a write weighting vector $\mathbf{w}_t^w \in \mathbb{R}^N$ is used to write information into the memory \mathbf{M}_t . First, information in the memory is erased with an erase vector $\mathbf{e}_t \in [0, 1]^W$, and subsequently added with a write vector $\mathbf{v}_t \in \mathbb{R}^W$

$$\mathbf{M}_t = \mathbf{M}_{t-1} \odot (\mathbf{E} - \mathbf{w}_t^w \mathbf{e}_t^\top) + \mathbf{w}_t^w \mathbf{v}_t^\top$$

where \odot denotes the element-wise matrix multiplication, and \mathbf{E} is an all-ones matrix of size $N \times W$.

The read and write weightings \mathbf{w}_t^r and \mathbf{w}_t^w are computed by read and write heads, respectively. These read and write heads support in total three memory attention mechanisms: (1) content-based writing and reading via a key/value mechanism, where the controller generates the keys, and attention weights are based on a similarity measure between a key and each memory slot; (2) writing via dynamic memory allocation; (3) sequential reading from memory slots in the forward or backward direction of previously written sequences. The read and write heads are controlled by the interface vector ξ_t , which the controller emits. ξ_t configures the memory attention mechanisms and contains the data to be written into the memory, and includes, e.g. the read/write keys or the write vector. The read/write heads compute then \mathbf{w}_t^r and \mathbf{w}_t^w based on ξ_t and the memory content (see [4] for details).

One often employs multiple read heads but only one write head. We change therefore for the remainder of the paper the indexing of the read weighting vector from \mathbf{w}_t^r to $\mathbf{w}_t^{r,i}$, and of the read vector from \mathbf{r}_t to \mathbf{r}_t^i , where i indexes the read head.

b) *DNC Controller*: The controller reads the input, accesses the memory, and produces the output of the DNC. The central part of the controller is the *controller network* which can be any ANN. In addition, the controller also includes linear transformations, \mathbf{W}_y , \mathbf{W}_r , and \mathbf{W}_ξ , which (1) generate the final DNC output, and (2) generate the interface vector ξ_t . Formally, the controller receives an input vector $\mathbf{x}_t \in \mathbb{R}^X$

and read vectors $\mathbf{r}_{t-1}^i \in \mathbb{R}^W$ from the previous time step of the R read heads and generates the final DNC output vector $\mathbf{y}_t \in \mathbb{R}^Y$ and interface vector ξ_t . For notational convenience, we concatenate the input vectors and memory readouts:

$$\chi_t = [\mathbf{x}_t; \mathbf{r}_{t-1}^1; \dots; \mathbf{r}_{t-1}^R]$$

with $\chi_t \in \mathbb{R}^{X+RW}$. The controller network processes the input χ_t and synchronously produces the controller network output $\mathbf{h}_t \in \mathbb{R}^H$ as $\mathbf{h}_t = ANN([\chi_1; \dots; \chi_t]; \theta)$, where ANN is any neural network (possibly recurrent) and θ are the network weights. The controller network output is then together with the read vectors linearly transformed to the final DNC output $\mathbf{y}_t \in \mathbb{R}^Y$:

$$\mathbf{y}_t = \mathbf{W}_y \mathbf{h}_t + \mathbf{W}_r [\mathbf{r}_t^1; \dots; \mathbf{r}_t^R] + \mathbf{b}_y$$

where \mathbf{W}_y is the so-called output matrix of size $Y \times H$, \mathbf{W}_r is the so-called readout matrix of size $Y \times RW$, and \mathbf{b}_y is a bias vector.

The interface vector ξ_t is computed as:

$$\xi_t = \mathbf{W}_\xi \mathbf{h}_t + \mathbf{b}_\xi$$

where \mathbf{W}_ξ is of size $(WR + 3W + 5R + 3) \times H$ and called interface matrix, and \mathbf{b}_ξ is the corresponding bias vector. ξ_t is interpreted by the read and write heads, and thus controls the memory attention mechanisms and the data written to and read from memory [4].

θ , $\mathbf{W}_{\{y,r,\xi\}}$ and $\mathbf{b}_{\{y,\xi\}}$ are usually found by an optimization algorithm.

III. APPROACHES

We introduce *compression* and *regularization* of the controller state-space as two approaches to facilitate input length generalization. We have analyzed our approaches in simple algorithmic tasks, and compared them with a stateful and a stateless controller as baselines. We describe in the following (A) the stateful baseline, (B) the architectural change underlying our approaches, (C and D) our approaches for state-space constraints, and (E) the stateless baseline.

A. Stateful Baseline

We employed an LSTM controller network [1] as a baseline in our experiments. An LSTM is stateful and thus enables the DNC to compute the output not only based on the input and the memory matrix but also based on the controller's state. We provide here the definition of the LSTM as used in our work:

$$\begin{aligned} \mathbf{i}_t &= \sigma(\mathbf{W}_i[\chi_t; \mathbf{h}_{t-1}] + \mathbf{b}_i) \\ \mathbf{f}_t &= \sigma(\mathbf{W}_f[\chi_t; \mathbf{h}_{t-1}] + \mathbf{b}_f) \\ \mathbf{o}_t &= \sigma(\mathbf{W}_o[\chi_t; \mathbf{h}_{t-1}] + \mathbf{b}_o) \\ \mathbf{c}_t &= \mathbf{f}_t \mathbf{c}_{t-1} + \mathbf{i}_t \tanh(\mathbf{W}_c[\chi_t; \mathbf{h}_{t-1}] + \mathbf{b}_c) \\ \mathbf{h}_t &= \mathbf{o}_t \tanh(\mathbf{c}_t) \end{aligned}$$

where σ is the logistic sigmoid function, and \mathbf{i}_t , \mathbf{f}_t , \mathbf{o}_t , \mathbf{c}_t , and $\mathbf{h}_t \in \mathbb{R}^H$ are the input gate, forget gate, output gate, cell state, and hidden state vectors, respectively, at time t . \mathbf{W}_i , \mathbf{W}_f , \mathbf{W}_o , $\mathbf{W}_c \in \mathbb{R}^{H \times (X+RW)}$, and \mathbf{b}_i , \mathbf{b}_f , \mathbf{b}_o , $\mathbf{b}_c \in \mathbb{R}^H$ are trainable weight matrices and bias vectors, respectively, and are referred to as θ in this work.

B. Peephole LSTM

Our compression and regularization approaches aim to constrain the state-space of the LSTM cell state \mathbf{c}_t . As an LSTM additionally contains a hidden state \mathbf{h}_t , our approaches could be rendered useless if state information is propagated unconstrainedly via the hidden state. However, we refrained from constraining the hidden state, as it is used to generate the interface vector ξ_t and could lead to impaired memory access. Instead, we (1) have adapted the LSTM so that only the cell state \mathbf{c}_t is propagated over time but not the hidden state \mathbf{h}_t , and (2) constrain only the cell state. Thus, the gates \mathbf{i}_t , \mathbf{f}_t , and \mathbf{o}_t have connections to \mathbf{c}_t instead of \mathbf{h}_t :

$$\begin{aligned} \mathbf{i}_t &= \sigma(\mathbf{W}_i[\chi_t; \mathbf{c}_{t-1}] + \mathbf{b}_i) \\ \mathbf{f}_t &= \sigma(\mathbf{W}_f[\chi_t; \mathbf{c}_{t-1}] + \mathbf{b}_f) \\ \mathbf{o}_t &= \sigma(\mathbf{W}_o[\chi_t; \mathbf{c}_{t-1}] + \mathbf{b}_o) \\ \mathbf{c}_t &= \mathbf{f}_t \mathbf{c}_{t-1} + \mathbf{i}_t \tanh(\mathbf{W}_c[\chi_t; \mathbf{c}_{t-1}] + \mathbf{b}_c) \\ \mathbf{h}_t &= \mathbf{o}_t \tanh(\mathbf{c}_t) \end{aligned}$$

This adapted LSTM corresponds to a Peephole LSTM [27], [28] where the gates have direct access, i.e. peepholes, to the cell state. In addition to standard Peephole LSTMs, we allow the \tanh activation function used in the cell state computation to access also the previous cell state.

C. State Compression

We speculated that limiting the range of possible state-space values could support the emergence of loops as the distances between different state vectors become potentially smaller, thus easing the learning of loops in the training phase (if the concrete algorithmic task can be solved with loops). In addition, such a limitation makes it also more probable that the controller operates within state-space regimes close to those it has been trained for. Instead of a hard value limit (i.e. clipping) which could impede gradient descent, we chose to compress the elements of the cell state vectors \mathbf{c}_t into the interval $(-1, 1)$ with the \tanh function. Based on the previously defined Peephole LSTM, we redefined \mathbf{c}_t and \mathbf{h}_t to implement state compression:

$$\begin{aligned} \tilde{\mathbf{c}}_t &= \mathbf{f}_t \mathbf{c}_{t-1} + \mathbf{i}_t \tanh(\mathbf{W}_c[\chi_t; \mathbf{c}_{t-1}] + \mathbf{b}_c) \\ \mathbf{c}_t &= \tanh(\tilde{\mathbf{c}}_t) \\ \mathbf{h}_t &= \mathbf{o}_t \tanh(\tilde{\mathbf{c}}_t) \end{aligned}$$

D. State Regularization

As an alternative to the compression of the state-space via the network architecture, state-space regularization penalizes distances between states that are already spatially close. It thus encourages revisiting of states and loops. We implemented state-space regularization by adding a regularization term to the loss function:

$$\mathcal{L} = \frac{1}{N} \sum_{i=1}^N (\alpha \mathcal{L}^i + (1 - \alpha) \mathcal{L}_{state}^i),$$

where N is the batch size, \mathcal{L}^i is either the mean square error (mse) or cross-entropy loss of the i -th training sample, \mathcal{L}_{state}^i

is the additional state-space regularization term, and α is a weighting coefficient. First, we calculated the cosine similarity between every cell state pair of the i -th training sample:

$$\cos(\mathbf{c}_x^i, \mathbf{c}_y^i) = \frac{\langle \mathbf{c}_x^i, \mathbf{c}_y^i \rangle}{\|\mathbf{c}_x^i\| \|\mathbf{c}_y^i\|}$$

Let π_x^i and π_y^i be two permutations of the cell state indices t for training sample i such that $\cos(\mathbf{c}_{\pi_x^i(1)}^i, \mathbf{c}_{\pi_y^i(1)}^i) \geq \cos(\mathbf{c}_{\pi_x^i(2)}^i, \mathbf{c}_{\pi_y^i(2)}^i) \geq \dots \geq \cos(\mathbf{c}_{\pi_x^i(n)}^i, \mathbf{c}_{\pi_y^i(n)}^i)$, where $\pi_x^i \neq \pi_y^i$. Next, we calculated the average of the K largest cosine similarities and transformed it into a loss:

$$\mathcal{L}_{state}^i = 1 - \frac{1}{K} \sum_{j=1}^K \cos(\mathbf{c}_{\pi_x^i(j)}^i, \mathbf{c}_{\pi_y^i(j)}^i)$$

The intention of considering only the K closest state pairs rather than all state pairs was to push states within a neighborhood closer to each other, but not states between neighborhoods, thus supporting the emergence of several clusters and subsequently loops.

E. Stateless Baseline

Our approaches to improve generalization require the existence of a state-space in the controller, and the vanilla LSTM controller is therefore an appropriate baseline. However, to embed our findings in a larger context, we performed experiments with a stateless controller network as a second baseline. For that purpose, we employed an feedforward neural network (FFNN) defined as following:

$$\mathbf{h}_t = FFNN_{\theta}(\chi_t),$$

where $FFNN_{\theta}()$ is a fully connected neural network with potentially multiple hidden layers and parameterized by θ .

IV. EXPERIMENTAL DESIGN AND ANALYSES

We conducted a series of tests to analyze the effectiveness of our proposed approaches for input-length generalization. Moreover, we analyzed their effects on the state-space of controller networks. In particular, we tested the compression, regularization, and baseline approaches with the following tasks: sort, copy, differentiation, shift, add, search, logic evaluation. All tasks were tested with five different controller networks: a Peephole LSTM with state compression, a Peephole LSTM with state regularization, a Peephole LSTM with state compression & state regularization, and – as baselines – an LSTM and an FFNN. We refer to the state compression and state regularization approaches as COMPR and REG, respectively, in our work. Their combination is termed COMPR®. We refer to the LSTM-based (stateful) and FFNN-based (stateless) controllers as STATEFUL-BASELINE and STATELESS-BASELINE, respectively.

Furthermore, we analyzed if a pre-trained DNC can be extended with a larger memory without retraining.

A. Tasks

The various tasks employed in the experiments and their respective description are provided in Table I; their implementation details can be found in Section Task Implementation Details in the supplementary materials. All tasks comprised an *encoding phase* and a *decoding phase*. In the encoding phase, the task-specific input was sequentially presented to the DNC, afterwards the task result was read out sequentially in the decoding phase. The search task additionally had a search query phase between the encoding and decoding phases (details in supplementary materials). Thus, the DNC received the complete task input for all tasks before any output was generated which required the DNC to utilize its memory. The total DNC input for all tasks comprised the task-specific input and a control channel separating the encoding and decoding phases. The total DNC output comprised the task result, and additionally, a signal channel indicating the end of the output for all tasks except the logic task.

B. Implementation

The employed LSTM and Peephole LSTM networks had 128 units; no stacking was used. For the FFNN, we set up three layers, each layer comprised 128 units, and a tanh activation function was used for the first two layers. Thus, all employed controller networks had an output size of $H = 128$. For the regularization approach, we set the weighting coefficient of the loss function to $\alpha = 0.9$, and we averaged the cosine similarities over the closest $K = 5$ states pairs. Those settings were found in preliminary experiments but were not systematically optimized. The neural networks were trained to minimize the mean squared error or, in the case of the logic evaluation task, the cross-entropy acquired in the decoding phase of the DNC output. The network training details can be found in Section Neural Network Training in the supplementary materials. To implement the experiments, we extended the original DNC available on GitHub¹ with our approaches. We used Python 3.7 (Python Software Foundation) and Tensorflow 1.15 (Google LLC). The extended DNC, our methods, the experiment framework, and the data are available on Zenodo².

C. Performance Analysis

We employed the *hit rate* for the search task and *classification accuracy* for all other tasks to quantify the performance. In more detail, we calculated the accuracy of a sample for the sort, copy, differentiation, shift, and add tasks by comparing the task result channel(s) of the DNC output with the respective target values and averaged over the duration of the decoding phase. For these tasks, we ignored the signal channel (which indicates the end of the output) as the output length was equal to the length of the input. For the logic evaluation task, we obtained a true/false value as a task result and calculated then the classification accuracy. For the search task, we obtained a sequence of position indices. The signal channel indicated the end of this sequence with a value above

¹<https://github.com/deepmind/dnc>

²<https://doi.org/10.5281/zenodo.5534734>

TABLE I
TASKS USED TO ANALYZE THE INPUT LENGTH GENERALIZATION ABILITY OF THE DNC. THE EXAMPLES SHOW THE INPUT AND OUTPUT OF THE DNC (THE EXAMPLES ARE SIMPLIFIED, THE CONTROL CHANNEL IS NOT SHOWN).

task	description	example
sort	sort a number sequence	$(2, 5, 2, 1, 3) \rightarrow (1, 2, 2, 3, 5)$
copy	output a received number sequence	$(2, 5, 2, 1, 3) \rightarrow (2, 5, 2, 1, 3)$
differentiation	output the absolute differences between successive numbers	$(2, 5, 2, 1, 3) \rightarrow (3, 3, 1, 2)$
shift	circular shift a number sequence by its half	$(2, 5, 2, 1, 3) \rightarrow (1, 3, 2, 5, 2)$
add	element-wise sum up two binary sequences	$((0, 1), (0, 0), (1, 1), (1, 0), (1, 0)) \rightarrow (1, 0, 2, 1, 1)$
search	output the relative positions of a queried numeral in a sequence	data: $(2, 5, 2, 1, 2)$, query: $(2) \rightarrow (0, 0.5, 1)$
logic evaluation	evaluate a propositional logic expression	$((\neg(T \wedge F) \rightarrow T) \vee F) \rightarrow T$

0.8. We calculated then the hit rate of the position indices, i.e. the ratio of the true position indices covered by the search result.

a) *Input Length Generalization*: For all investigated approaches and tasks, we trained a DNC first with samples comprising training input sequences ranging in length from $N_{in} = 5$ to 15. Afterward, we evaluated the generalization performance with test input sequences ranging in length from $N_{in} = 2$ to 100. We generated 10 batches for each evaluated input length and evaluated the performance. We used a batch size of 64, and obtained in total 640 samples per evaluated sequence length. Subsequently, we averaged the classification accuracy or hit rate over all samples. We refer to such a training and evaluation cycle of a particular generalization approach and task as a trial. Eventually, we conducted 10 trials with different weight initializations for each task and generalization approach.

b) *Memory Extension*: Even if a DNC has perfect input-length generalization, its memory capacity can limit the length of the processable sequences (in particular, if the entire sequence needs to be stored in memory). However, a large memory is not always an option as the training time increases with the memory size, or the required memory may be incorrectly estimated and designed too small. To save computational resources or spare re-training with a sufficiently large memory, one might want to increase the memory size after training the DNC. We tested if our generalization approaches are compatible with this idea, and analyzed the performance of the DNC after replacing the memory M of a pre-trained DNC with a 10 times larger memory of size $N = 500$. We evaluated the performance then for input sequence lengths ranging from $N_{in} = 2$ to 1000, analogously to the evaluation described above. To account for the increased computational load in the inference phase, we evaluated the performance with 3 instead of 10 batches. Furthermore, we evaluated the performance not at every single sequence length but in intervals that got progressively larger from 5 to 100.

D. State-Space Analysis

We visualized the development of the controller states over time. For that purpose, we fed the trained networks an input sequence of length 30. We selected test input lengths beyond the maximum training length of $N_{in} = 15$ to observe the state-space behavior when generalization is required. Thus, latest with time step 16, the network showed state transitions that evolved due to the intrinsic network dynamics. To allow for

a fair comparison between the approaches, we tapped into the controllers' cell state output before applying a potential state compression function (\tanh), i.e. we used \tilde{c}_t with COMPR and COMPR®, and c_t with STATEFUL-BASELINE and REG. We then recorded the state-space during the processing of the input sequences, and subsequently reduced the dimensionality of the 128 hidden states to two dimensions to allow visual inspection of the state-space dynamics. For dimensionality reduction, we employed t-distributed stochastic neighbor embedding (t-SNE) [29], which is especially suited to visualize potential clusters in high-dimensional data. We used the t-SNE implementation of the Python scikit-learn toolbox 0.23.1 (perplexity was set to 50; we used default settings for other parameters).

E. Memory Attention Mechanism Analysis

The employed DNC supports two memory attention mechanisms for writing (content-based addressing and dynamic memory allocation) and two for reading (content-based addressing and backward/forward sequential addressing). We analyzed if our proposed generalization approaches affect the employed memory attention mechanisms. For that purpose, we calculated the histograms of the so-called *allocation gate* and *read mode vector*, which the DNC derives from the interface vector ξ_t (see [4] for details). The results can be found in supplementary materials in Section Memory Attention Mechanisms.

V. RESULTS

A. DNC Performance

We evaluated the performance of our proposed generalization approaches with input lengths N_{in} ranging from 2 to 100. Note that we trained with input lengths ranging from 5 to 15. We employed hit rate for the search task and classification accuracy for all other tasks to quantify the performance. Fig. 1 shows the task performance vs the input length. We show the median over 10 trials for each generalization approach (solid line), and additionally the trials with the maximum average performance between $N_{in} = 2$ and $N_{in} = 45$ (dashed lines). Table II shows the maximum processable input lengths for our generalization approaches and the baselines. The maximum processable input length was defined as the maximum input length for which the trials' median was above a performance of 95%. Furthermore, we calculated the average performance between $N_{in} = 2$ and $N_{in} = 45$ for each trial and provide descriptive statistics wrt. trials in Table III.

Additionally, we compared the generalization approaches with a non-parametric statistical test (Mann-Whitney U test), see Table IV. To account for multiple comparisons, we adjusted the p -values with the false discovery rate (FDR) method [30] and consider p -values ≤ 0.05 as statistically significant.

a) Performance of compression and regularization:

The compression and regularization approaches featured a better input length generalization than the stateful baseline for the sort, copy, and differentiation tasks (c.f. COMPR/REG/COMPR® vs STATEFUL-BASELINE in Fig. 1 and Table III). In particular, for the sort and copy tasks our approaches allowed input sequences twice as long as the stateful baseline, and 1.4 times longer for the differentiation task (c.f. Table II). When comparing between our approaches, COMPR® yielded a better generalization than the individual approaches, COMPR and REG, for the sort, copy, and differentiation tasks. For the sort and differentiation tasks, the differences between COMPR, REG, or COMPR® compared to STATEFUL-BASELINE were statistically significant, as well as the differences between REG or COMPR® compared to STATEFUL-BASELINE for the copy task (Mann-Whitney U test with FDR correction, c.f. Table IV). A statistically significant difference has moreover been found between COMPR® and REG in the differentiation task.

For the remaining 4 tasks, i.e. shift, add, logic evaluation, and search, Fig. 1 and Tables II and III show that our compression and regularization approaches have similar performances to the stateful baseline. With the add task, REG, COMPR®, and STATEFUL-BASELINE generalized similarly, whereas COMPR generalized slightly better. With the shift and search tasks, no apparent input length generalization was observed for any approach. With the logic evaluations task, a limited generalization beyond the training input lengths can be observed. Several statistically significant differences have been found with the Mann-Whitney U test between the approaches (c.f. Table IV), however, Fig. 1 suggests that the differences were mainly in regions with low performance. An exception is the add task with COMPR vs REG, with a distinct difference also in regions with high performance.

Our generalization approaches are based on a Peephole LSTM to prevent the unconstrained propagation of the hidden state over time. For comparison purposes, we implemented the generalization approaches additionally with a vanilla LSTM and evaluated the performance on the sort task, see Section LSTM vs Peephole LSTM in the supplementary materials. Indeed, the generalization performance considerably decreased when using state compression or state regularization with a vanilla LSTM. Furthermore, without using state compression or state regularization, the Peephole LSTM yielded a similarly poor generalization performance as the vanilla LSTM. Thus, the Peephole LSTM alone does not feature generalization capabilities but enables the generalization effect of state compression/regularization.

b) Performance of the stateless controller: Also, the stateless controller improved the input length generalization of the DNC. With the sort and differentiation task, it generalized better than the LSTM-based controller (stateful baseline) but

worse than the compression or regularization approaches (c.f. Fig. 1 and Table II). However, a statistically significant difference has only been found in the sort task for COMPR® compared to STATELESS-BASELINE.

With the copy task, the stateless controller generalized best, although not statistically different from the compression or regularization approaches. With the add task, the generalization of the stateless controller was similar to the other approaches, and no statistically significant differences have been found to other approaches. However, the stateless controller achieved only a suboptimal performance with the shift, logical evaluation, and search tasks.

c) Best performing trials: We show the trials with the largest average performance in the interval $N_{in} = 2$ to $N_{in} = 45$ as dashed lines in Fig. 1, and provide the maximum values in Table III. The best trials of the COMPR, COMPR®, and STATELESS-BASELINE approaches achieved an accuracy of 100 % between $N_{in} = 2$ to $N_{in} = 45$ for the sort, copy, differentiation and add tasks. For the sort and copy tasks, the best trial of the stateful baseline achieved a generalization performance worse than even the trial median of any other approach. Also with the add task, the best stateful baseline trial generalized worse than the other best trials. However, for the differentiation task, the situation was inverted, and the best trial of the stateful baseline was superior to the other trials.

TABLE II
MAXIMUM INPUT LENGTHS WITH A MEDIAN TASK PERFORMANCE ABOVE 95 % (HIT RATE FOR SEARCH, OTHERWISE CLASSIFICATION ACCURACY).
THE BEST APPROACHES ARE BOLD.

tasks	STATEFUL-BASELINE	STATELESS-BASEL.	COMPR	REG	COMPR®
sort	23	39	45	46	48
copy	17	41	36	35	39
differentiation	24	31	35	34	37
shift	16	8	16	16	16
add	40	43	46	39	41
logic eval.	32	0	27	31	29
search	18	6	18	17	17

B. DNC Performance with Extended Memory

Next, we analyzed the performance of the DNC after replacing the memory of a pre-trained DNC with a 10 times larger memory of size $N = 500$. Note that we trained the DNC only with input lengths ranging from 5 to 15. Fig. 2 shows the task performance of input sequence lengths ranging from $N_{in} = 2$ to $N_{in} = 1000$, and Table V shows the maximum input lengths with a median task performance over 95 %. Further analyses, analogously to the previous section, can be found in the supplementary materials in Section DNC Performance with Extended Memory. The combined compression and regularization approach yielded a distinctively better generalization performance due to the memory extension for the copy, differentiation, and add task (c.f. Table II vs Table V). In particular, with the add task, the high performance lasted close to the new memory limit of $N = 500$. A special case is the sort task: the median performance dropped from ca. 100 % to 90 %; however, this 90 % performance plateau was observed to last close to the new memory limit. In stark contrast, the generalization performance of the stateful and stateless baselines dropped considerably for most tasks due to the

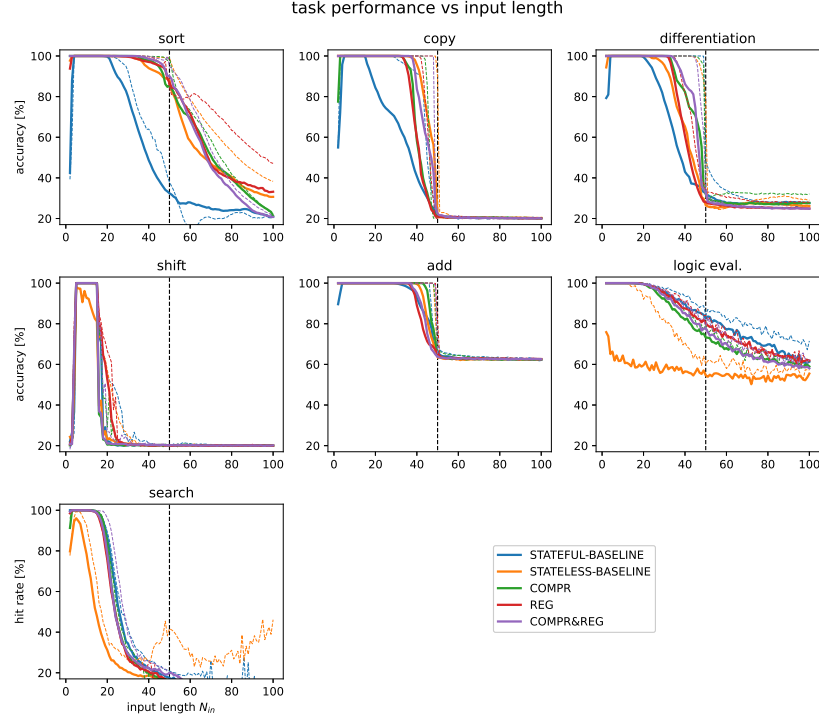


Fig. 1. Performance of the various generalization approaches vs the input length, shown for each task. Solid lines show the medians over 10 trials, and dashed lines show the best trials (i.e. with a maximum average performance from $N_{in} = 2$ to 45). The dashed vertical line marks the number of memory slots (i.e. 50). Note that we trained with input lengths ranging from $N_{in} = 5$ to 15.

TABLE III

DESCRIPTIVE STATISTICS OF THE TASK PERFORMANCE OVER TRIALS (HIT RATE FOR SEARCH, OTHERWISE CLASSIFICATION ACCURACY IN %). THE LARGEST MEDIAN VALUES ARE BOLD.

tasks	STATEFUL-BASELINE				STATELESS-BASELINE				COMPR				REG				COMPR®			
	median	max	mean	SD	median	max	mean	SD	median	max	mean	SD	median	max	mean	SD	median	max	mean	SD
sort (acc)	81	86	80	4	98	100	98	2	99	100	98	2	99	100	93	9	99	100	99	0
copy (acc)	74	95	74	17	97	100	88	21	90	100	90	6	91	99	90	5	95	100	94	6
differentiation (acc)	80	100	78	14	88	100	84	19	93	100	94	5	90	95	90	3	96	100	92	12
shift (acc)	45	50	45	3	40	50	37	11	42	46	43	1	48	51	48	2	42	47	41	5
add (acc)	98	100	95	6	99	100	94	11	100	100	99	1	97	100	97	2	98	100	98	2
logic eval. (acc)	96	98	96	1	60	87	62	14	94	95	93	1	96	97	96	1	95	96	95	1
search (hit rate)	63	66	63	2	41	50	41	5	61	64	60	2	60	61	58	2	60	68	60	4

TABLE IV

APPROACHES COMPARED WITH A MANN-WHITNEY U TEST AND FDR CORRECTED p -VALUES. STATISTICALLY SIGNIFICANT DIFFERENCES ARE BOLD ($p \leq 0.05$).

tasks	STATEFUL-BASELINE vs				STATELESS-BASELINE vs			COMPR vs		REG vs	
	STATELESS-BASELINE	COMPR	REG	COMPR®	COMPR	REG	COMPR®	REG	COMPR®	COMPR®	
sort	0.00	0.00	0.02	0.00	0.19	0.48	0.03	0.15	0.46	0.10	
copy	0.03	0.07	0.05	0.02	0.14	0.14	0.41	0.48	0.13	0.10	
differentiation	0.19	0.03	0.05	0.05	0.09	0.40	0.10	0.08	0.48	0.03	
shift	0.14	0.03	0.05	0.05	0.42	0.03	0.46	0.00	0.44	0.00	
add	0.44	0.15	0.48	0.21	0.21	0.30	0.38	0.03	0.31	0.33	
logic eval.	0.00	0.01	0.22	0.09	0.00	0.00	0.00	0.00	0.03	0.08	
search	0.00	0.07	0.00	0.09	0.00	0.00	0.00	0.09	0.48	0.21	

memory extension. The generalization performance improved slightly only for the add task and the stateful baseline. Thus, both baselines learned to a large extent a controller strategy dependent on the memory size, whereas the compression and regularization approach allowed to learn a more independent strategy. For the shift, logic evaluation, and search tasks, all approaches achieved a suboptimal generalization performance – similar to the previous section.

The best trials' performances show that the stateful baseline could also learn a control strategy that generalizes (c.f. copy, differentiation and add tasks in Fig. 2). However, a

strategy featuring generalization was more frequent for the compression and regularization approach as indicated by the trial medians.

C. Controller States

Fig. 3 and 4 depict the state-space trajectories of the encoding phases for the sort and copy tasks. In the sort task, the LSTM-based controller (STATEFUL-BASELINE) featured cell states which evolved along a steady progressing trajectory (see Fig. 3). Thus, the controller did not revisit states, and every new time step pushed the controller cell state into a

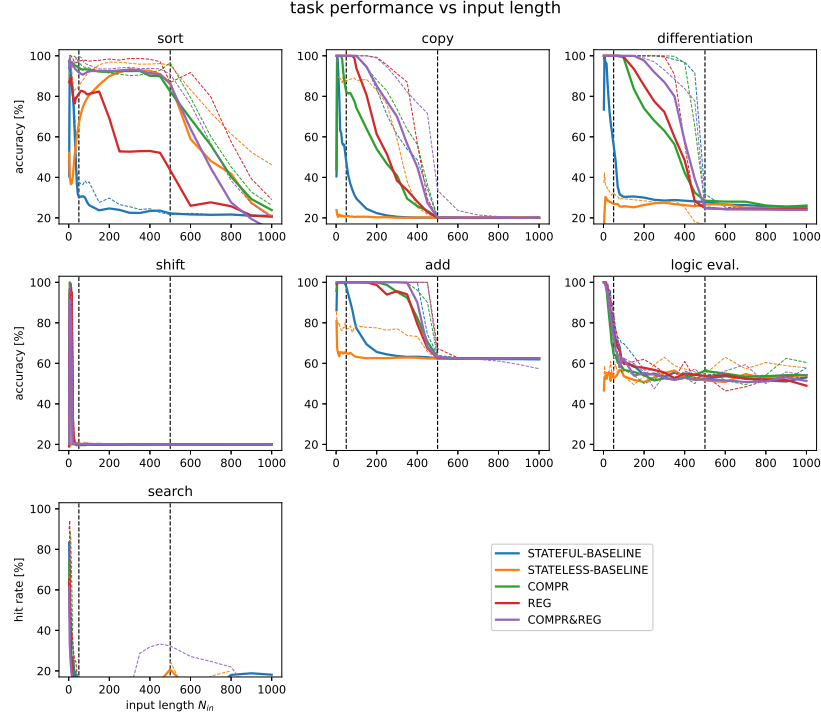


Fig. 2. DNC with memory extension, and the performance of the various generalization approaches vs the input length shown for each task. Solid lines show the medians over 10 trials, and dashed lines show the best trials (i.e. with a maximum average performance from $N_{in} = 2$ to 450). The dashed vertical lines mark the number of original and extended memory slots, 50 and 500, respectively. Note that we trained with input lengths ranging from $N_{in} = 5$ to 15.

TABLE V

DNC WITH MEMORY EXTENSION: MAXIMUM INPUT LENGTHS WITH A MEDIAN TASK PERFORMANCE ABOVE 95 % (HIT RATE FOR SEARCH, OTHERWISE CLASSIFICATION ACCURACY). THE BEST APPROACHES ARE BOLD.

tasks	STATEFUL-BASELINE	STATELESS-BASELINE	COMPR	REG	COMPR®
sort	10	0	40	0	15
copy	10	0	35	100	150
differentiation	20	0	150	150	250
shift	15	0	15	15	0
add	60	0	350	250	400
logic eval.	25	0	20	25	20
search	0	0	0	0	0

new region of the state-space. Furthermore, the trajectories started from a common point but drifted away from each other during processing. On the contrary, state compression (COMPR) yielded salient state-space clusters revisited during processing. Thus, state compression was accompanied by loops in the state-space. Furthermore, the different samples ended up in a small state-space region, suggesting an orderly transition from the encoding to the decoding phase. Moreover, five apparent clusters emerged during the encoding phase in all shown COMPR trials, corresponding to the encoding of the five possible input numerals. The state-space resulting from the state regularization approach (REG) appears less consistent across trials. The best performing trial showed a cluster structure similar to the COMPR trials (i.e. containing loops). The second best-performing trial, showed a new structure comprising five clusters associated with five initial states, and a common end state. Depending on the first input numeral, the controller entered one of those five clusters and operated within a cluster. The worse performing trials featured

a steady progressing trajectory comparable to STATEFUL-BASELINE. However, two of them (99 % and 83 %) showed a more regular spacing between subsequent states, and also did not drift away from each other towards the end of the encoding phase. Moreover, all REG trials except the worst performing converged into a small state-space region at the end of the encoding phase, allowing for a controlled transition into the decoding phase. The combination of state compression and regularization (COMPR®) also featured a wide variety of state-space patterns. Noteworthy, all trials yielded a nearly perfect accuracy, and one cannot relate a specific pattern to a certain accuracy range. The two best performing trials showed a mixture of (1) states that evolved along a steady progressing trajectory, and (2) state changes between clusters along these trajectories. Three other trials showed five large clusters with loops between states, and one trial showed five detached clusters, which were entered at the beginning of the input phase. All trials converged at the end of the encoding phase into a small state-space region.

In the copy task, STATEFUL-BASELINE featured a steady progressing trajectory for all trials, similar to the sort task. Notable, the three STATEFUL-BASELINE trials with a high performance showed a distinctive convergence point separated from the rest of the trajectory. In contrast, the trials of the other methods featuring high performance, i.e. COMPR, REG, and COMPR®, showed a highly structured and clustered state-space containing loops. Interestingly, some of these trials had five distinctive clusters, some had five larger clusters but contained smaller clusters within them (e.g. COMPR with 93 % or REG with 99 %), and some comprised

of more than five clusters. Interestingly, trials with a low performance featured steady progressing trajectories similar to the STATEFUL-BASELINE trials.

One can find the plots of the encoding phase for the remaining tasks in the supplementary materials in Section Controller States. The differentiation and add tasks showed state-space trajectories qualitatively similar to the sort and copy tasks. Thus, trials yielding a high performance also showed a highly structured and clustered state-space supporting the emergence of loops. Some trials reached a perfect accuracy even with STATEFUL-BASELINE, and featured then a highly structured state-space with loops. However, COMPR, REG, and COMPR® yielded a highly structured and clustered state-space in some search task trials but without any concomitant generalization improvement. This indicates that a high generalization performance often paralleled loops in the state-space, but loops alone were not sufficient for generalization.

Furthermore, state-space differences were present in the decoding phase (see plots in supplementary materials in Section Controller States). In the sort task, the generalization approaches induced clusters in the state-space but these cluster were mostly visited sequentially. The differences are more apparent with the copy, differentiation, and add tasks: COMPR induced loops in the state-space, whereas REG and COMPR® often caused the state-space to converge into a small region only after a few time steps. Thus, state regularization enforced in these cases a solution with a minimal movement through the state-space (which is in the extreme case analogous to STATELESS-BASELINE).

VI. DISCUSSION

We introduced state-space compression and state-space regularization as a possibility to improve the input length generalization of the DNC. On three tasks (sort, copy, differentiation), our compression and regularization approaches reached distinctively higher classification accuracies than the stateful baseline controller (LSTM) when input length generalization was required. Interestingly, the performance of the stateless baseline controller (FFNN) was on par with our approaches in 3 tasks (sort, copy, add), and only slightly lower in the differentiation task. However, for other tasks (shift, logic evaluation, search), the stateless baseline controller failed to obtain a reasonable performance even for sequence lengths seen in the training phase. While the stateful baseline performed well for all evaluated tasks for known sequence lengths, it failed to generalize to novel sequence lengths in most tasks. Our introduced compression and regularization approaches, however, combine the advantages of both baselines. They featured generalization in some tasks but never failed to learn the sample distribution provided in the training phase.

With some of our tasks, we observed that the performance started to decrease quickly with a sequence length close to 50. As this limit corresponded to the number of memory slots employed in our networks, we particularly suspected the memory size as a limiting factor for the generalization performance. However, increasing the memory size increases

also the computational costs, which is especially undesirable in the training phase. We tested therefore a computationally cheaper and practically relevant alternative to overcome the memory limit: we replaced the memory of a *pre-trained* network with a larger one. This allowed us to solve 4 tasks with considerably longer input sequences, especially when combining the compression and regularization approaches. As the memory size was increased by a factor of 10, one could also expect a similar increase in the length of processable input sequences. Interestingly, we observed a smaller increase which was furthermore task-dependent. One reason for that might be accumulated noise introduced by each memory access operation [22]. In striking contrast to our generalization approaches, both baselines failed to generalize or perform at all with the extended memory.

Our intuition behind compression and regularization was that they could introduce an inductive bias towards compacter state-spaces, allowing the controller to re-use states instead of drifting off into novel state-space regimes. This could lead to the formation of loops in the state-space of the controller. Notably, this is exactly what we have observed for the sort, copy, differentiation, and add tasks, especially in the encoding phases. However, also the stateful baseline had state-space loops in the add task, although only for trials with a high generalization performance. Furthermore, the compression and regularization approaches featured loops in the search task without being attended by generalization. Thus, state-space loops were often but not in all tasks associated with a better generalization performance. Our introduced compression and regularization approaches facilitated such structures but were not necessary for them to emerge, nor were state-space loops sufficient for generalization. Whether loops paralleled generalization depended on the concrete task. This raises the question of which algorithmic element state-space loops realize. One can observe that many state-space plots show loops over exactly as many clusters as input numerals. Thus, every input numeral was probably processed by a specific cluster. This is analogous to a loop over switch-case blocks in an algorithm. Thus, our compression and regularization approaches may especially learn well algorithms comprising of such blocks. However, other algorithmic elements needed to solve, for example, the logic evaluation task cannot be learned efficiently; the DNC learns instead shortcuts between input/output pairs that do not generalize to out-of-distribution examples. Such other algorithmic elements could be, for example, subprograms [15], [18] or recursion [31], which both have been shown to benefit generalization.

The original NTM [7] already had the capability of input length generalization for some algorithmic tasks (e.g. copy task) without any explicit generalization approach. Also we found the stateful baseline to produce generalizing solutions sometimes. However, our generalization approaches produce more often solutions that can generalize. Furthermore, the limitations of the NTM compared to the DNC may have facilitated generalizing solutions for some cases. For example, Taguchi and Tsuruoka [20] have shown that the performance can be improved by excluding the controller output when calculating the final output of the DNC or NTM. Moreover,

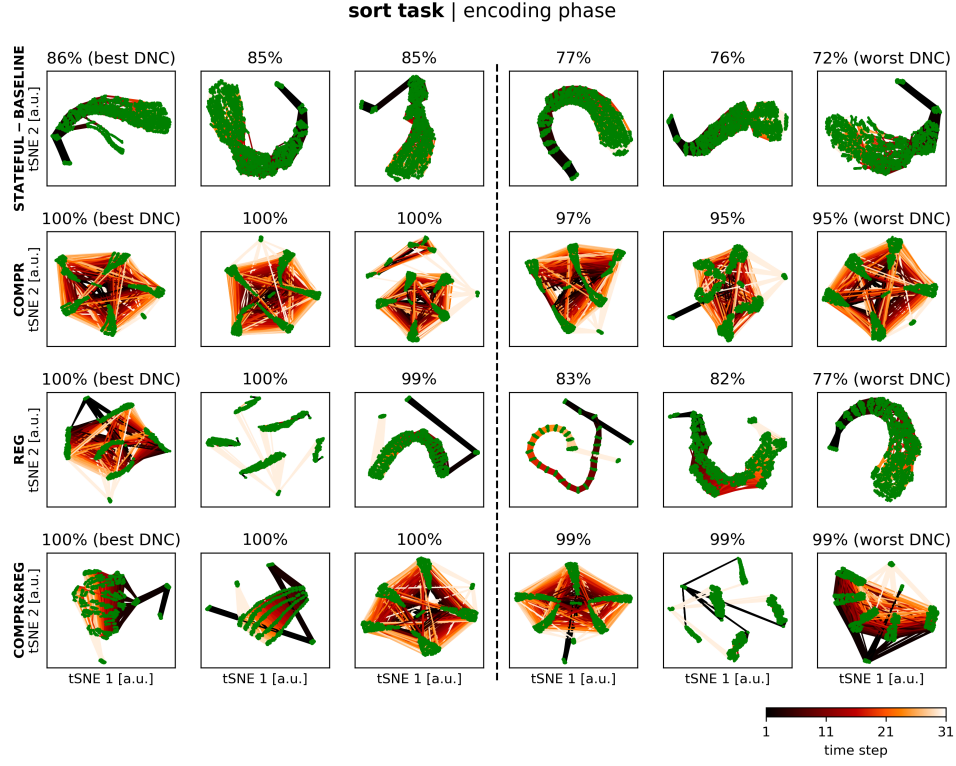


Fig. 3. Cell state trajectories from the encoding phase of the sort task projected with t-SNE. Shown are the three best and three worst performing networks for each generalization approach (wrt. the average performance for input lengths between 2 and 45) on the left and right half, respectively. The trajectories show the processing of a sequence of length 30 and the end-of-input flag. The cell states are marked as green dots with color-coded transitions (from dark to light in the direction of processing). We show overlaid trajectories of 64 samples for each trial.

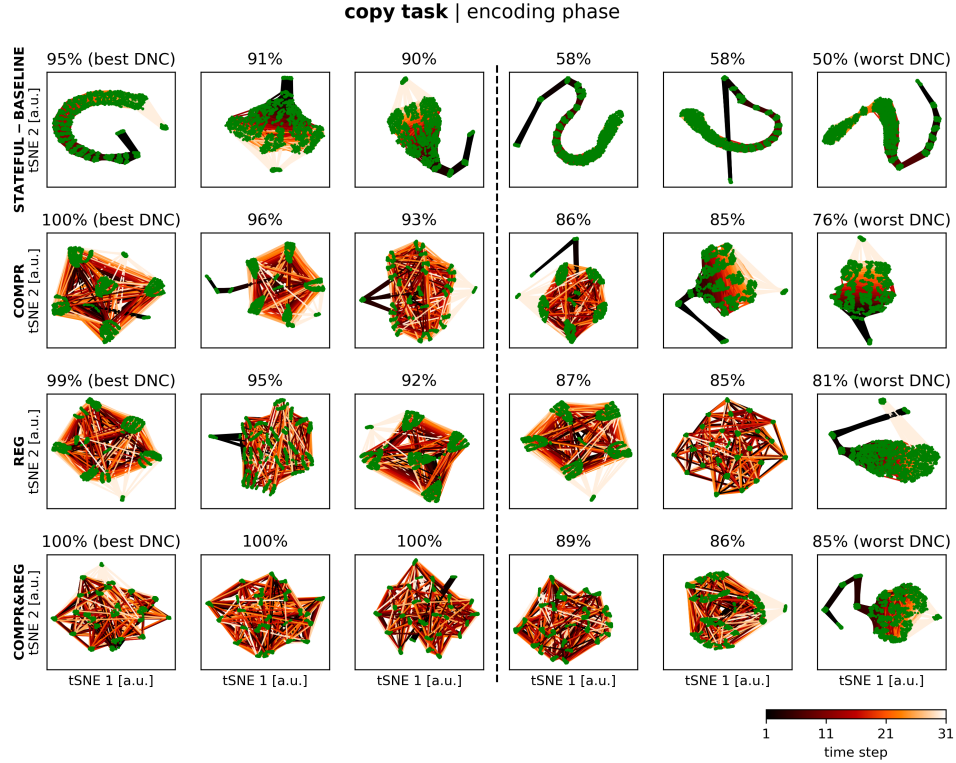


Fig. 4. Cell state trajectories from the encoding phase of the copy task projected with t-SNE.

Rae et al. [19] have shown that sparse memory access can lead to input-length generalization in an associative recall task. Thus, model limitations – like our compression approach – can sometimes be beneficial for generalization.

In general, performance comparisons between the individual approaches are difficult as the employed tasks or their concrete instantiations differed. However, our compression and regularization approaches are orthogonal to the existing methods and could be used in addition. Our approaches are, in principle, applicable for any MANN with a controller.

Our approaches also have limitations. First of all, it is difficult to prove that the DNC has indeed learned an algorithm with state compression/regularization. The DNC could also have learned a strategy to process samples drawn from the training dataset distribution and gained robustness by compression/regularization. However, robustness alone would not allow generalization to arbitrary-sized input sequences (given a sufficiently large memory). Second, our approaches do not provide a general solution for input-length generalization. Whether they lead to a generalizing solution depends on the concrete task and its underlying algorithm. Third, we solely focused on input-length generalization. Whether our approaches are also beneficial for other types of generalization was not investigated. Finally, the time complexity of the state regularization approach is $\mathcal{O}(t^2)$, with t being the number of time steps. This is due to the calculation of the cosine similarity between every state pair. While this may not be necessarily problematic in practice, one should research heuristics to reduce the number of compared state pairs.

VII. CONCLUSION AND FUTURE WORK

We have demonstrated that our approaches for state-space constraints, namely compression and regularization, improve the input-length generalization of the DNC for some algorithmic tasks. These approaches are not limited to the DNC but apply to any MANN with a stateful controller. In particular, our approaches allow training a MANN with shorter input sequences, which (1) saves computational resources, and (2) facilitates training when long training input sequences are expensive to obtain. Furthermore, our approaches allow to simply extend the memory after the training phase to increase input-length generalization when memory is a limiting factor. Interestingly, we have observed that loop-like structures in the state-space often occur together with input-length generalization. They suggest a link to loops in algorithms, and that especially this algorithmic element can be well learned through our state-space compression and regularization approaches.

Future work should find a comprehensive categorization of algorithmic tasks which an MANN can learn while featuring generalization. Furthermore, it should be analyzed whether the current approaches introduce only robustness or if they have the potential for a theoretically unlimited and error-less generalization.

ACKNOWLEDGMENT

Know-Center is funded by the Austrian COMET Program – Competence Centers for Excellent Technologies – under the

auspices of the Austrian Federal Ministry for Climate Action, Environment, Energy, Mobility, Innovation and Technology, the Austrian Federal Ministry for Digital and Economic Affairs, and by the state of Styria. COMET is managed by the Austrian Research Promotion Agency (FFG). The authors thank Joana Pereira for helpful comments on the manuscript.

REFERENCES

- [1] S. Hochreiter and J. Schmidhuber, “Long short-term memory,” *Neural Computation*, vol. 9, no. 8, pp. 1735–1780, 1997.
- [2] W. Zaremba and I. Sutskever, “Learning to execute,” 2014, 1410.4615.
- [3] N. Kalchbrenner, I. Danihelka, and A. Graves, “Grid long short-term memory,” in *4th International Conference on Learning Representations, ICLR 2016, San Juan, Puerto Rico, May 2-4, 2016, Conference Track Proceedings* (Y. Bengio and Y. LeCun, eds.), 2016, 1507.01526.
- [4] A. Graves, G. Wayne, M. Reynolds, T. Harley, I. Danihelka, A. Grabska-Barwińska, S. G. Colmenarejo, E. Grefenstette, T. Ramalho, J. Agapiou, A. P. Badia, K. M. Hermann, Y. Zwols, G. Ostrovski, A. Cain, H. King, C. Summerfield, P. Blunsom, K. Kavukcuoglu, and D. Hassabis, “Hybrid computing using a neural network with dynamic external memory,” *Nature*, vol. 538, no. 7626, pp. 471–476, 2016.
- [5] H. T. Siegelmann and E. D. Sontag, “On the computational power of neural nets,” *Journal of Computer and System Sciences*, vol. 50, no. 1, pp. 132–150, 1995.
- [6] D. Bahdanau, K. Cho, and Y. Bengio, “Neural machine translation by jointly learning to align and translate,” in *3rd International Conference on Learning Representations, ICLR 2015, San Diego, CA, USA, May 7-9, 2015, Conference Track Proceedings* (Y. Bengio and Y. LeCun, eds.), 2015, 1409.0473.
- [7] A. Graves, G. Wayne, and I. Danihelka, “Neural Turing machines,” 2014, 1410.5401.
- [8] S. Sukhbaatar, A. Szlam, J. Weston, and R. Fergus, “End-to-end memory networks,” in *Advances in Neural Information Processing Systems 28: Annual Conference on Neural Information Processing Systems 2015, December 7-12, 2015, Montreal, Quebec, Canada* (C. Cortes, N. D. Lawrence, D. D. Lee, M. Sugiyama, and R. Garnett, eds.), pp. 2440–2448, 2015.
- [9] A. Joulin and T. Mikolov, “Inferring algorithmic patterns with stack-augmented recurrent nets,” in *Advances in Neural Information Processing Systems* (C. Cortes, N. Lawrence, D. Lee, M. Sugiyama, and R. Garnett, eds.), vol. 28, Curran Associates, Inc., 2015.
- [10] Y. Ma and J. C. Principe, “A taxonomy for neural memory networks,” *IEEE Transactions on Neural Networks and Learning Systems*, vol. 31, no. 6, pp. 1780–1793, 2020.
- [11] O. Vinyals, M. Fortunato, and N. Jaitly, “Pointer networks,” in *Advances in Neural Information Processing Systems* (C. Cortes, N. Lawrence, D. Lee, M. Sugiyama, and R. Garnett, eds.), vol. 28, Curran Associates, Inc., 2015.
- [12] L. Kaiser and I. Sutskever, “Neural gpus learn algorithms,” in *4th International Conference on Learning Representations, ICLR 2016, San Juan, Puerto Rico, May 2-4, 2016, Conference Track Proceedings* (Y. Bengio and Y. LeCun, eds.), 2016, 1511.08228.
- [13] T. Huynh, M. Maire, and M. R. Walter, “Multigrid neural memory,” in *Proceedings of the 37th International Conference on Machine Learning, ICML 2020, 13-18 July 2020, Virtual Event*, vol. 119 of *Proceedings of Machine Learning Research*, pp. 4561–4571, PMLR, 2020.
- [14] A. Goyal, A. Lamb, J. Hoffmann, S. Sodhani, S. Levine, Y. Bengio, and B. Schölkopf, “Recurrent independent mechanisms,” 2019, 1909.10893.
- [15] S. E. Reed and N. de Freitas, “Neural programmer-interpreters,” in *4th International Conference on Learning Representations, ICLR 2016, San Juan, Puerto Rico, May 2-4, 2016, Conference Track Proceedings* (Y. Bengio and Y. LeCun, eds.), 2016, 1511.06279.
- [16] K. Kurach, M. Andrychowicz, and I. Sutskever, “Neural random-access machines,” in *4th International Conference on Learning Representations, ICLR 2016, San Juan, Puerto Rico, May 2-4, 2016, Conference Track Proceedings* (Y. Bengio and Y. LeCun, eds.), 2016, 1511.06392.
- [17] C. Li, D. Tarlow, A. L. Gaunt, M. Brockschmidt, and N. Kushman, “Neural program lattices,” in *5th International Conference on Learning Representations, ICLR 2017, Toulon, France, April 24-26, 2017, Conference Track Proceedings*, OpenReview.net, 2017.

- [18] Y. Yan, K. Swersky, D. Koutra, P. Ranganathan, and M. Hashemi, "Neural execution engines: Learning to execute subroutines," in *Advances in Neural Information Processing Systems 33: Annual Conference on Neural Information Processing Systems 2020, NeurIPS 2020, December 6-12, 2020, virtual* (H. Larochelle, M. Ranzato, R. Hadsell, M. Balcan, and H. Lin, eds.), 2020.
- [19] J. W. Rae, J. J. Hunt, I. Danihelka, T. Harley, A. W. Senior, G. Wayne, A. Graves, and T. Lillicrap, "Scaling memory-augmented neural networks with sparse reads and writes," in *Advances in Neural Information Processing Systems 29: Annual Conference on Neural Information Processing Systems 2016, December 5-10, 2016, Barcelona, Spain* (D. D. Lee, M. Sugiyama, U. von Luxburg, I. Guyon, and R. Garnett, eds.), pp. 3621–3629, 2016.
- [20] N. Taguchi and Y. Tsuruoka, "Partially non-recurrent controllers for memory-augmented neural networks," 2018, 1812.11485.
- [21] J. Franke, J. Niehues, and A. Waibel, "Robust and scalable differentiable neural computer for question answering," 2018, 1807.02658.
- [22] R. Csordás and J. Schmidhuber, "Improving differentiable neural computers through memory masking, de-allocation, and link distribution sharpness control," in *7th International Conference on Learning Representations, ICLR 2019, New Orleans, LA, USA, May 6-9, 2019*, OpenReview.net, 2019.
- [23] T. Park, I. Choi, and M. Lee, "Distributed memory based self-supervised differentiable neural computer," vol. abs/2007.10637, 2020, 2007.10637.
- [24] H. Le, T. Tran, and S. Venkatesh, "Neural stored-program memory," in *8th International Conference on Learning Representations, ICLR 2020, Addis Ababa, Ethiopia, April 26-30, 2020*, OpenReview.net, 2020.
- [25] H. Le and S. Venkatesh, "Neurocoder: Learning general-purpose computation using stored neural programs," vol. abs/2009.11443, 2020, 2009.11443.
- [26] G. Yang and A. M. Rush, "Lie-access neural turing machines," in *5th International Conference on Learning Representations, ICLR 2017, Toulon, France, April 24-26, 2017, Conference Track Proceedings*, OpenReview.net, 2017.
- [27] F. A. Gers, N. N. Schraudolph, and J. Schmidhuber, "Learning precise timing with LSTM recurrent networks," *J. Mach. Learn. Res.*, vol. 3, pp. 115–143, 2002.
- [28] H. Sak, A. W. Senior, and F. Beaufays, "Long short-term memory recurrent neural network architectures for large scale acoustic modeling," in *INTERSPEECH 2014, 15th Annual Conference of the International Speech Communication Association, Singapore, September 14-18, 2014* (H. Li, H. M. Meng, B. Ma, E. Chng, and L. Xie, eds.), pp. 338–342, ISCA, 2014.
- [29] L. van der Maaten and G. Hinton, "Visualizing data using t-sne," *Journal of Machine Learning Research*, vol. 9, no. 86, pp. 2579–2605, 2008.
- [30] Y. Benjamini and Y. Hochberg, "Controlling the false discovery rate: A practical and powerful approach to multiple testing," *Journal of the Royal Statistical Society: Series B (Methodological)*, vol. 57, no. 1, pp. 289–300, 1995.
- [31] J. Cai, R. Shin, and D. Song, "Making neural programming architectures generalize via recursion," in *5th International Conference on Learning Representations, ICLR 2017, Toulon, France, April 24-26, 2017, Conference Track Proceedings*, OpenReview.net, 2017.
- [32] D. P. Kingma and J. Ba, "Adam: A method for stochastic optimization," in *3rd International Conference on Learning Representations, ICLR 2015, San Diego, CA, USA, May 7-9, 2015, Conference Track Proceedings* (Y. Bengio and Y. LeCun, eds.), 2015, 1412.6980.
- [33] Y. LeCun, L. Bottou, G. B. Orr, and K. R. Müller, "Efficient backprop," in *Lecture Notes in Computer Science*, pp. 9–50, Springer Berlin Heidelberg, 1998.
- [34] X. Glorot and Y. Bengio, "Understanding the difficulty of training deep feedforward neural networks," in *Proceedings of the Thirteenth International Conference on Artificial Intelligence and Statistics, AISTATS 2010, Chia Laguna Resort, Sardinia, Italy, May 13-15, 2010* (Y. W. Teh and D. M. Titterton, eds.), vol. 9 of *JMLR Proceedings*, pp. 249–256, JMLR.org, 2010.
- [35] R. Pascanu, T. Mikolov, and Y. Bengio, "On the difficulty of training recurrent neural networks," in *International conference on machine learning*, pp. 1310–1318, 2013.

SUPPLEMENTARY MATERIALS

A. Task Implementation Details

a) *sort, copy, differentiation, and shift tasks*: For these four tasks, the input to the DNC was a two-dimensional vector sequence $\mathbf{x}_t \in \mathbb{R}^2$. The first dimension of \mathbf{x}_t corresponded to the actual task input in_t , the second dimension was a control channel ctr_t indicating the end of the task input. The output of the DNC was also a two-dimensional vector $\mathbf{y}_t \in \mathbb{R}^2$, where the first dimension corresponded to the actual task result out_t and the second dimension was a signal channel sig_t indicating the end of the DNC output. The DNC received first the task input in_t for N_{in} time steps (with $in_t = 0, \forall t > N_{in}$). Right after the total task input was presented to the DNC (i.e. the input was encoded), the control channel ctr_t was set to 1.0 at $t = N_{in} + 1$ and to 0.0 everywhere else. This was the so-called *end-of-input flag* which indicated the end of the task input and the encoding phase, and switched the DNC into the decoding phase. The task result out_t was then decoded by the DNC for N_{out} time steps, i.e. from $t = N_{in} + 2$ to $t = N_{in} + 1 + N_{out}$. The DNC was trained to set the signal channel sig_t to 1.0 at $t = N_{in} + 1 + N_{out} + 1$, and to 0.0 before this time, corresponding to the *end-of-output flag*. For the considered tasks the task result had the same length as the task input, i.e. $N_{out} = N_{in}$ (for the differentiation task, we prepended a constant symbol to the task result). Thus, the total number of time steps to fully process the tasks accumulated to $N_{total} = N_{in} + 1 + N_{out} + 1 = 2N_{in} + 2$.

We evaluated these tasks with a base-5 numeral system, i.e. a quinary system, comprising numerals 0 to 4. These numerals were not used directly as task input in_t but normalized to the interval $[-1.0, 1.0]$ before. Moreover, we normalized the target for the task result out_t to the same interval in the training phase. In the evaluation phase, out_t was de-normalized and rounded.

b) *add task*: The add task was implemented using three-dimensional input and output vector sequences $\mathbf{x}_t \in \mathbb{R}^3$ and $\mathbf{y}_t \in \mathbb{R}^3$. Analogous to the tasks described previously, the last dimension of \mathbf{x}_t and \mathbf{y}_t corresponded to the control channel ctr_t and signal channel sig_t , respectively. The first two dimensions of \mathbf{x}_t encompassed the two task input sequences $in_{1,t}$ and $in_{2,t}$ which had to be added by the DNC. It was a binary add task, and the binary numerals 0 and 1 were encoded as -1.0 and 1.0, respectively, in $in_{1,t}$ and $in_{2,t}$. The first two dimensions of \mathbf{y}_t encompassed the up to two digits binary addition result ranging from 00 to 10 (the output numerals 0 and 1 were again encoded as -1.0 and 1.0, respectively). The control channel ctr_t and the signal channel sig_t were employed like in the tasks described above and marked the end of the encoding and decoding phases. Analogously, the total number of time steps for the add task was $N_{total} = 2N_{in} + 2$.

c) *search task*: The search task consisted of three phases: encoding, search query, and decoding. In the encoding phase, an input sequence in_t based on five numerals (0 to 4) was presented to the DNC. Subsequently, the search query q corresponding to one out of the five numerals was presented. Eventually, the DNC returned the positions out_t of the queried numerals within the input sequence.

The total input to the DNC was a two-dimensional vector sequence $\mathbf{x}_t \in \mathbb{R}^2$ where the first dimension contained the input sequence in_t with a length of N_{in} followed by a blank and the search query q at $t = N_{in} + 2$. Like in the, e.g. sort task, the numerals were normalized to the interval $[0.0, 1.0]$. The second dimension contained the control channel ctr_t . The control channel ctr_t marked the end of the input sequence in_t as well as the end of the search query q with a value of 1.0 and was set to 0.0 otherwise. The DNC output was also a two-dimensional vector sequence $\mathbf{y}_t \in \mathbb{R}^2$ comprising the actual search results out_t and the signal channel sig_t marking the end of the output. Starting from $t = N_{in} + 4$, out_t yielded the found positions of q , with one position per time step. The positions were normalized to the interval $[0.0, 1.0]$, corresponding to the begin and end of in_t , respectively. With N_{out} being the number of found positions, the total number of time steps for the search task was $N_{total} = N_{in} + 3 + N_{out} + 1$.

d) *logic evaluation task*: The DNC was trained to parse a propositional logic formula and infer its truth value. For the sake of implementation we did not use proposition symbols, e.g. the A and B in $\neg(A \wedge B)$ but used true/false values (\top, \perp) instead. The problem of defining propositions and assigning logical values to them was out of scope for this task and we focused on the actual evaluation of a logic formula. A logical formula in our logic task was for example: $((\neg(\top \wedge \perp) \rightarrow \top) \vee \perp) \leftrightarrow \top$, which evaluates to \top (true).

The input $\mathbf{x}_t \in \mathbb{R}^{10}$ to the DNC comprised a vector $in_t \in \mathbb{R}^9$ representing the logic formula of length N_{in} and a control channel ctr_t separating encoding and decoding phases as in the preceding tasks. We used an one-hot encoding for in_t to represent logical values (\top, \perp), operators ($\neg, \vee, \wedge, \rightarrow, \leftrightarrow$) and parentheses. The truth value of the logic formula was encoded in the DNC output $\mathbf{y}_t \in \mathbb{R}$ at $t = N_{in} + 2$ as 0.0 or 1.0. The total number of time-steps for this task was $N_{total} = N_{in} + 2$.

B. Neural Network Training

All tasks but logic evaluation were set up as regression problems, where we used the mean squared error (MSE) as a loss function to be minimized by the training algorithm. We averaged the MSE over all dimensions of the DNC output \mathbf{y}_t and the relevant time steps of the decoding phase containing the task result, i.e. $N_{total} - N_{out} \leq t \leq N_{total}$. The logic evaluation task was set up as a classification problem, where we used the cross-entropy as loss function for $\mathbf{y}_{N_{total}}$. For each task, we generated task-specific training samples $(\mathbf{x}_t, \mathbf{y}_t)$ programmatically during the training phase. The input length N_{in} of the generated training samples ranged from 5 to 15 (uniformly distributed between batches, but equal for all samples within a batch).

We trained the LSTM, Peephole LSTM, or FFNN-based controllers separately for each task using backpropagation with ADAM [32]. We set the learning rate and other ADAM specific parameters to the values suggested in [32], in particular, the learning rate was set to $\alpha = 0.001$. The training encompassed the controller network parameters θ , the output/readout/interface matrices $\mathbf{W}_{\{y,r,\xi\}}$ with $\mathbf{b}_{\{y,\xi\}}$, and, if applicable, the initial states \mathbf{h}_0 and \mathbf{c}_0 of the controller

network. We initialized the parameters θ of the LSTM-based controllers and the output/readout/interface matrices with the LeCun method [33]. For the FFNN, we used the Glorot method [34]. We drew the values of the initial cell and hidden state vectors from a centered normal distribution with unit standard deviation. To prevent the exploding gradient problem, we applied gradient clipping [35].

Using a batch size of 64, we trained the DNC controllers for 300 000 iterations. Every 10th iteration, we computed the loss of the DNC using an input length $N_{in} = 30$ to estimate the generalization or out-of-distribution performance. We calculated then a running average over the last 500 out-of-distribution losses. Eventually, we selected the DNC at the iteration with the lowest averaged out-of-distribution loss for further evaluation.

C. LSTM vs Peephole LSTM

We qualitatively assessed the importance of the Peephole LSTM, which is supposed to prevent the unconstrained propagation of the hidden state over time. For this purpose, we evaluated the sort task performance when combining compression and regularization with a vanilla LSTM instead of a Peephole LSTM, and show the results in Fig. 5. The plot indicates that the architecture of the Peephole LSTM is indeed important for our generalization approaches (at least in the sort task) as only the combination of the Peephole LSTM and state compression or regularization considerably improved the generalization performance.

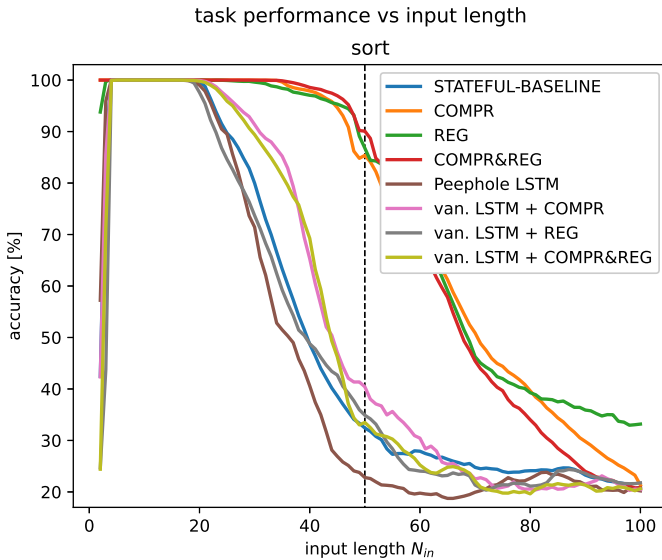


Fig. 5. Performance on the sort task when combining the state constraints approaches with a Peephole LSTM (COMPR, REG, COMPR®, as in the main paper) and a vanilla LSTM (van. LSTM + approach). Furthermore, the performances of the Peephole LSTM and the vanilla LSTM without any state constraints are shown (STATEFUL-BASELINE and Peephole LSTM).

D. DNC Performance with Extended Memory

Table VI shows descriptive statistics of the trial performances averaged between $N_{in} = 2$ to 450. We also conducted

Mann-Whitney U tests on the averaged trial performances, and provide the FDR corrected p -values in Table VII.

E. Memory Attention Mechanisms

The employed DNC supports two memory attention mechanisms for writing (i.e. content-based addressing and dynamic memory allocation) and two for reading (i.e. content-based addressing and backward/forward sequential addressing). The DNC learns to use and combine the attention mechanisms to solve a task. We analyzed if our proposed generalization approaches affect the learned memory attention mechanisms. We calculated the histograms of the allocation gate and read mode vector. Both vectors are computed at each time step from the interface vector ξ_t , see [4] for details. The allocation gate sets the ratio between content-based addressing (values close to 0) and dynamic memory allocation (values close to 1) when writing to memory. The read mode vector comprises of three components specifying the ratio between forward sequential addressing, backward sequential addressing, and content-based addressing. We evaluated here only the content-based addressing component, where values close to 1 correspond to content-based addressing, and values close to 0 correspond to sequential addressing in any direction when reading from memory. We refer to the allocation gate value as *write mode*, and to the value of the content-based addressing component of the read mode vector as *read mode* (i.e. g_t^a and $\pi_t^i[2]$, respectively, in [4]). We analyzed exemplarily the sort and copy tasks, and show the histograms of the read/write modes for STATEFUL-BASELINE, STATELESS-BASELINE, COMPR, REG, and, COMPR® in Figures 6 – 9. The figures show the histograms computed from the three best and three worst performing networks (w.r.t. the average performance on the input length interval 2 to 45). The actual histogram values were calculated based on an input length of $N_{in} = 15$, and are shown separately for the encoding and decoding phases. The read modes from the four read heads were aggregated.

With STATEFUL-BASELINE and the sort task, one can observe that the two write modes were often intermixed. Thus, content-based addressing and dynamic memory allocation were used simultaneously when accessing the memory. The encoding and decoding phases showed here a similar behavior. However, the other methods – which also yielded a better generalization performance – showed a clear separation between the two write modes. With them, the DNC used predominantly dynamic memory allocation during the encoding phase and content-based writing during the decoding phase. The read mode showed a similar behavior: the read modes of STATEFUL-BASELINE were intermixed, whereas the read modes of the other methods were well separated. The methods except STATEFUL-BASELINE used predominantly sequential reading during the encoding phase and content-based reading during the decoding phase. This could reflect a strategy where the DNC monotonously stored the input data via dynamic memory allocation during the encoding phase and did the actual sorting task in the decoding phase as indicated by content-based reading and writing. Furthermore, it is observable that networks trained with methods other than STATEFUL-BASELINE also tended to intermixed read/write modes when

TABLE VI

DNC WITH MEMORY EXTENSION AND DESCRIPTIVE STATISTICS OF THE TASK PERFORMANCE OVER TRIALS (HIT RATE FOR SEARCH, OTHERWISE CLASSIFICATION ACCURACY IN %). THE LARGEST MEDIAN VALUES ARE BOLD.

tasks	STATEFUL-BASELINE				STATELESS-BASELINE				COMPR				REG				COMPR®			
	median	max	mean	SD	median	max	mean	SD	median	max	mean	SD	median	max	mean	SD	median	max	mean	SD
sort (acc)	42	48	41	6	66	91	68	17	93	96	89	10	74	98	68	23	91	96	88	10
copy (acc)	48	89	51	20	21	79	30	18	69	91	70	16	82	94	79	12	89	96	86	11
differentiation (acc)	52	99	59	21	26	31	27	3	88	98	79	18	90	94	80	16	94	97	83	23
shift (acc)	30	32	30	2	20	20	20	0	28	30	29	2	30	32	30	2	28	30	27	2
add (acc)	85	99	85	11	64	77	64	10	96	99	96	2	93	100	93	7	98	100	98	2
logic eval. (acc)	75	78	74	2	54	56	53	4	70	71	70	1	74	78	73	3	73	75	72	3
search (hit rate)	19	23	18	3	11	43	15	12	15	26	16	4	15	24	15	4	11	16	12	3

TABLE VII

DNC WITH MEMORY EXTENSION AND APPROACHES COMPARED WITH A MANN-WHITNEY U TEST AND FDR CORRECTED p -VALUES. STATISTICALLY SIGNIFICANT DIFFERENCES ARE BOLD ($p \leq 0.05$).

tasks	STATEFUL-BASELINE vs				STATELESS-BASELINE vs			COMPR vs		REG vs	
	STATELESS-BASELINE	COMPR	REG	COMPR®	COMPR	REG	COMPR®	REG	COMPR®	COMPR®	COMPR®
sort	0.00	0.00	0.04	0.00	0.01	0.34	0.01	0.03	0.48	0.04	
copy	0.01	0.07	0.01	0.00	0.00	0.00	0.00	0.22	0.04	0.06	
differentiation	0.00	0.04	0.03	0.05	0.00	0.00	0.00	0.41	0.38	0.09	
shift	0.00	0.06	0.38	0.01	0.00	0.00	0.00	0.06	0.13	0.01	
add	0.00	0.06	0.12	0.02	0.00	0.00	0.00	0.16	0.12	0.03	
logic eval.	0.00	0.00	0.34	0.07	0.00	0.00	0.00	0.03	0.03	0.12	
search	0.15	0.06	0.03	0.00	0.30	0.32	0.48	0.34	0.04	0.11	

the achieved performance was low. Thus, the intermixing of access modes was associated with the STATEFUL-BASELINE method and/or suboptimal performance.

An intermixing of read and write modes can also be observed for the copy task in most networks with low performance. For networks with high performance, the write mode during the encoding phase was predominantly dynamic memory allocation. However, for the decoding phase, the dynamic memory allocation was often mixed with content-based addressing. This was reversed for the read mode. During the encoding phase, content-based addressing was often intermixed with sequential addressing; and during the decoding phase, mostly sequential addressing was used. A predominant usage of dynamic memory allocation during the encoding phase and sequential reading during the decoding phase suggests a monotonic memory access strategy during both phases and is expected with a copy task.

To conclude, controller networks with a high generalization performance often had constant ratios of the respective memory access modes (i.e. distinctive peaks in the histograms). Thus, their memory access patterns were rather stable and little dependent on the actual input data. In contrast, controller networks with a low generalization performance often exhibited ratios more spread. Thus, their memory access modes varied throughout the encoding and decoding phases. This could indicate a non-robust controller behavior highly tuned to the training data set, preventing generalization.

F. Controller States

Figures 10 to 19 show the trajectories of the controller states for all tasks (except the decoding phase of the sort and copy tasks, which were presented in the main paper). The decoding phase state plots were omitted for the logic evaluation and search task because the former has inconsistent decoding phase lengths between samples, and the latter comprises only one decoding phase time step. The trajectories show the processing of an input sequence with length 30 and the end-of-input

or end-of-output flag for the encoding or decoding phase, respectively.

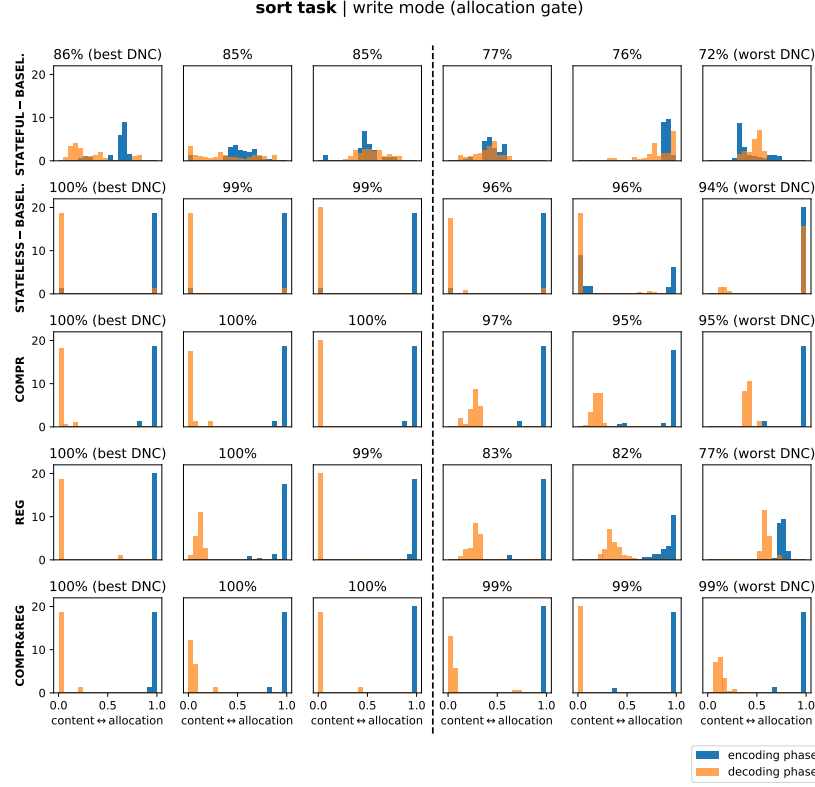


Fig. 6. Sort task write modes: Histograms of allocation gate values for input length $N_{in} = 15$. Left/right half: trials with best/worst performance. Values close to 0 indicate content-based addressing, values close to 1 indicate dynamic memory allocation. The encoding and decoding phases are shown separately.

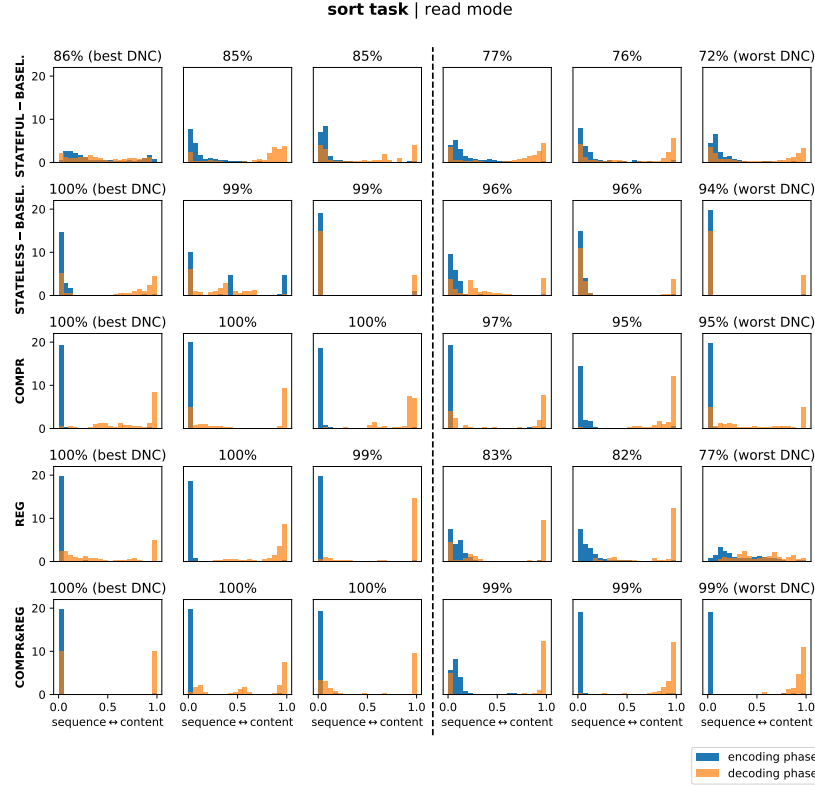


Fig. 7. Sort task read modes: Histograms of read mode values for input length $N_{in} = 15$. Left/right half: trials with best/worst performance. Values close to 0 indicate sequential addressing (forward or backward), values close to 1 indicate content-based addressing. The encoding and decoding phases are shown separately.

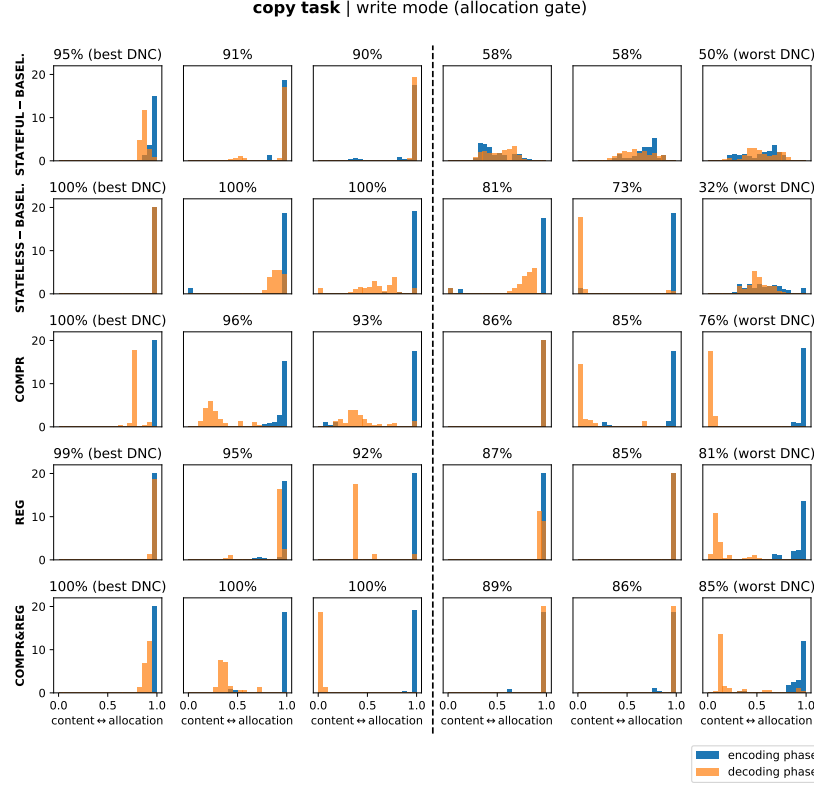


Fig. 8. Copy task write modes: Histograms of allocation gate values for input length $N_{in} = 15$. Left/right half: trials with best/worst performance. Values close to 0 indicate content-based addressing, values close to 1 indicate dynamic memory allocation. The encoding and decoding phases are shown separately.

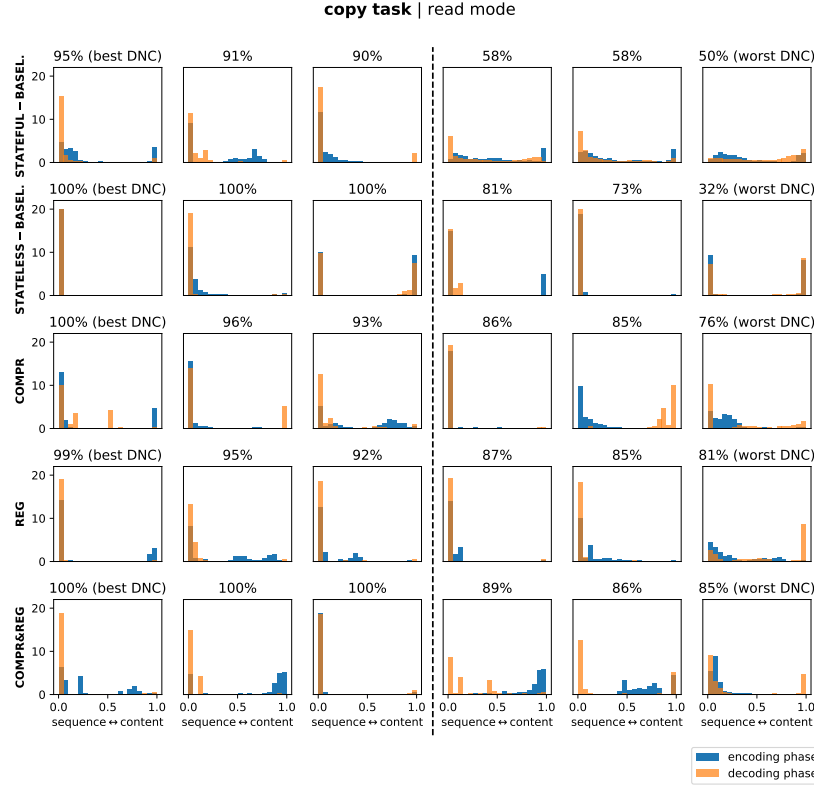


Fig. 9. Copy task read modes: Histograms of read mode values for input length $N_{in} = 15$. Left/right half: trials with best/worst performance. Values close to 0 indicate sequential addressing (forward or backward), values close to 1 indicate content-based addressing. The encoding and decoding phases are shown separately.

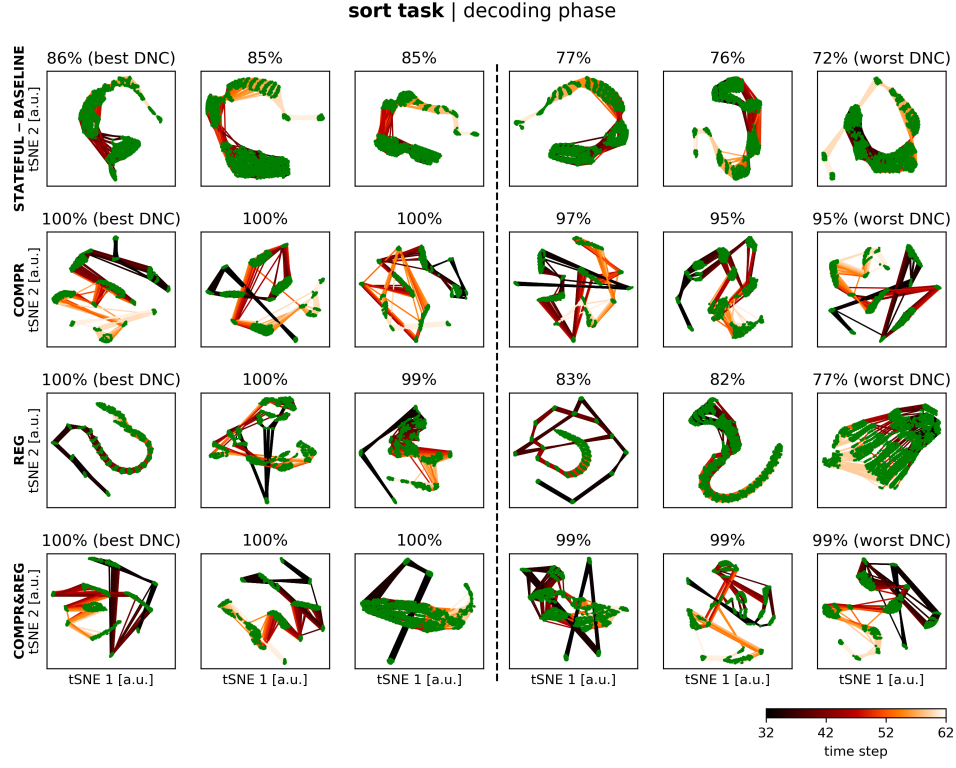


Fig. 10. Cell state trajectories from the decoding phase of the sort task projected with t-SNE. The trajectories show the processing of a sequence of length 30 and the end-of-output flag. The cell states are marked as green dots with color-coded transitions (from dark to light in the direction of processing). We show overlaid trajectories of 64 samples for each network.

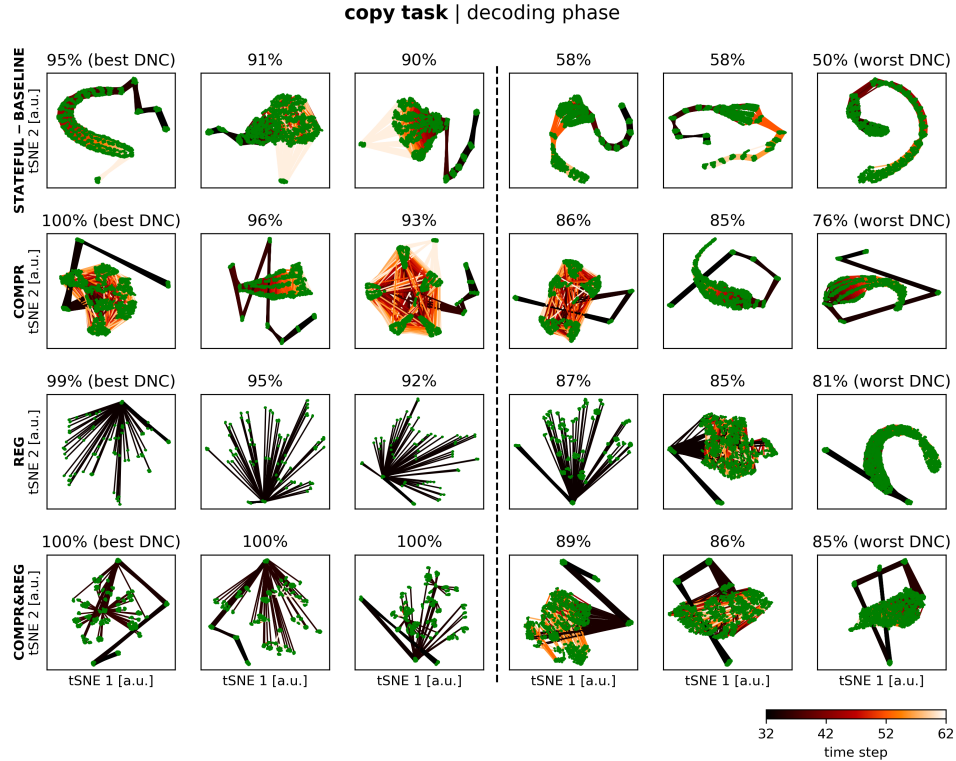


Fig. 11. Cell state trajectories from the decoding phase of the copy task projected with t-SNE.

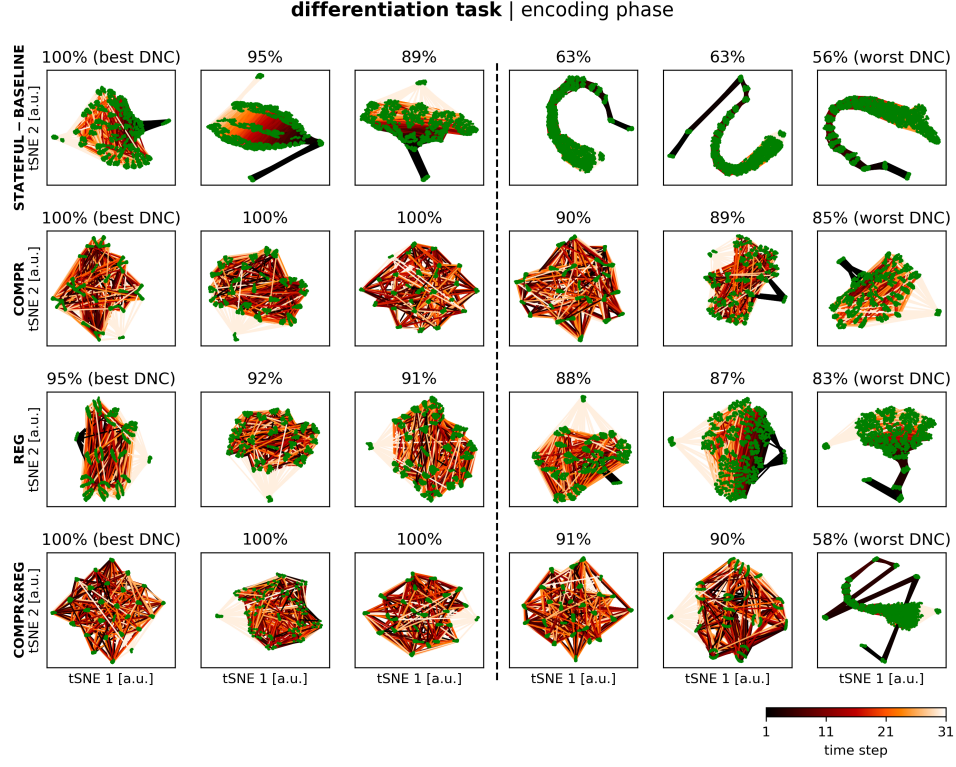


Fig. 12. Cell state trajectories from the encoding phase of the differentiation task projected with t-SNE. The trajectories show the processing of a sequence of length 30 and the end-of-input flag.

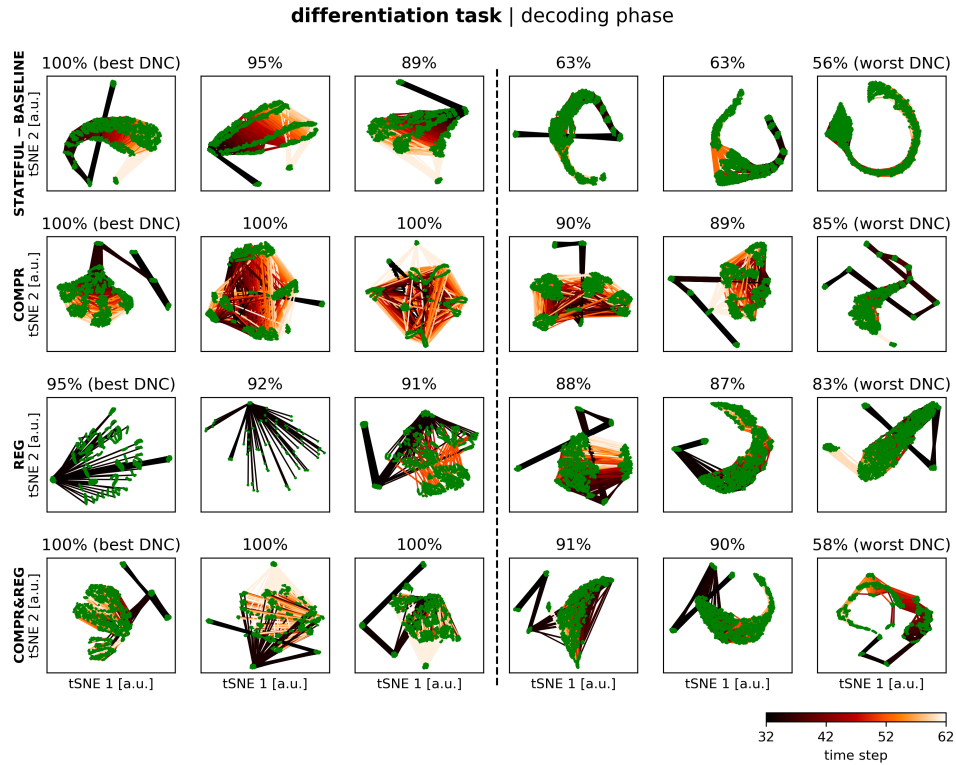


Fig. 13. Cell state trajectories from the decoding phase of the differentiation task projected with t-SNE.

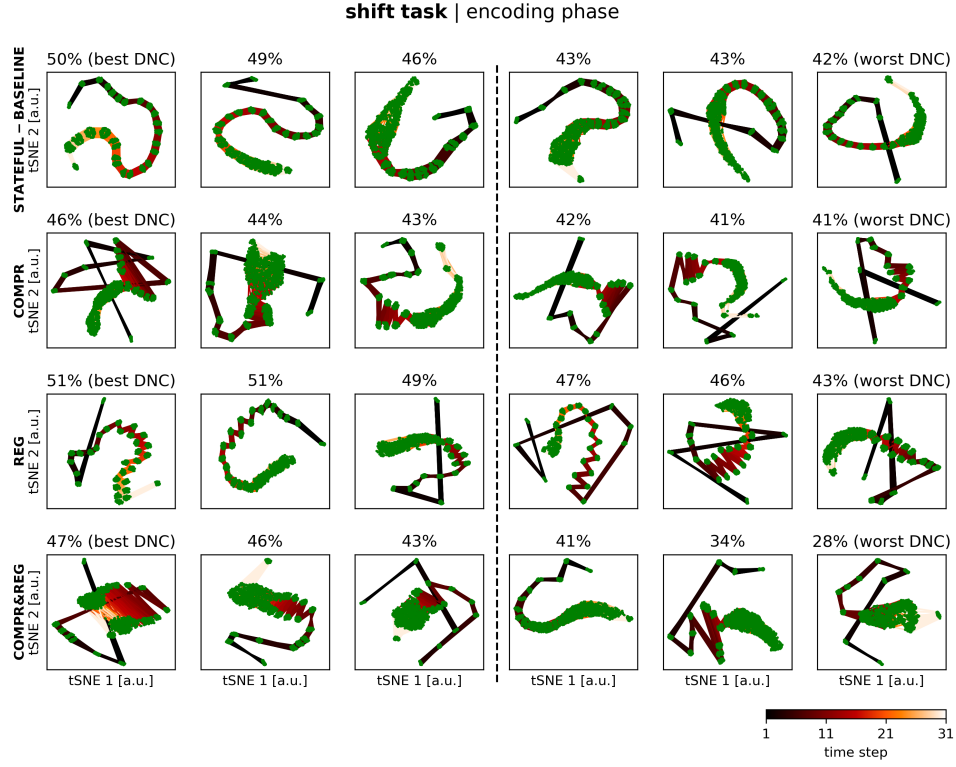


Fig. 14. Cell state trajectories from the encoding phase of the shift task projected with t-SNE.

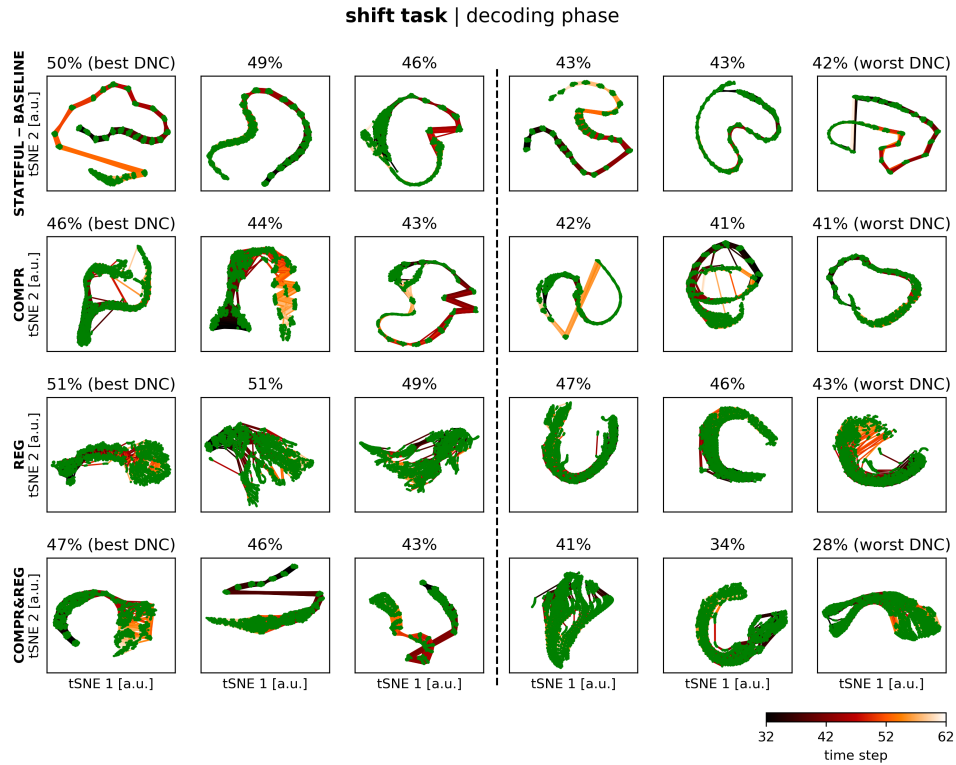


Fig. 15. Cell state trajectories from the decoding phase of the shift task projected with t-SNE.

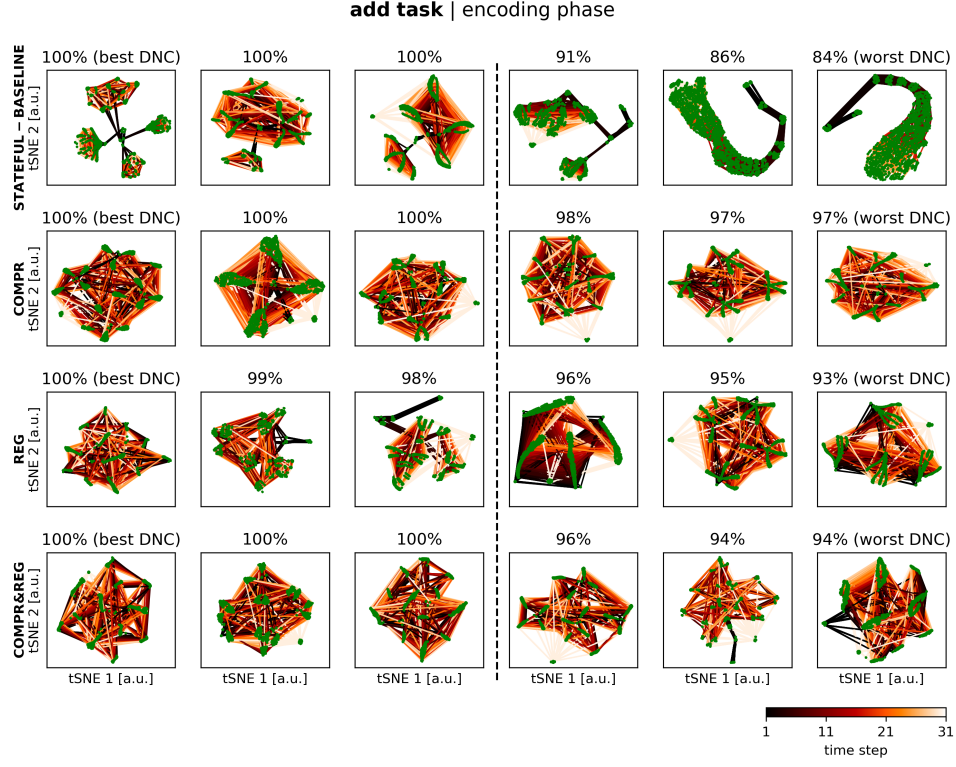


Fig. 16. Cell state trajectories from the encoding phase of the add task projected with t-SNE.

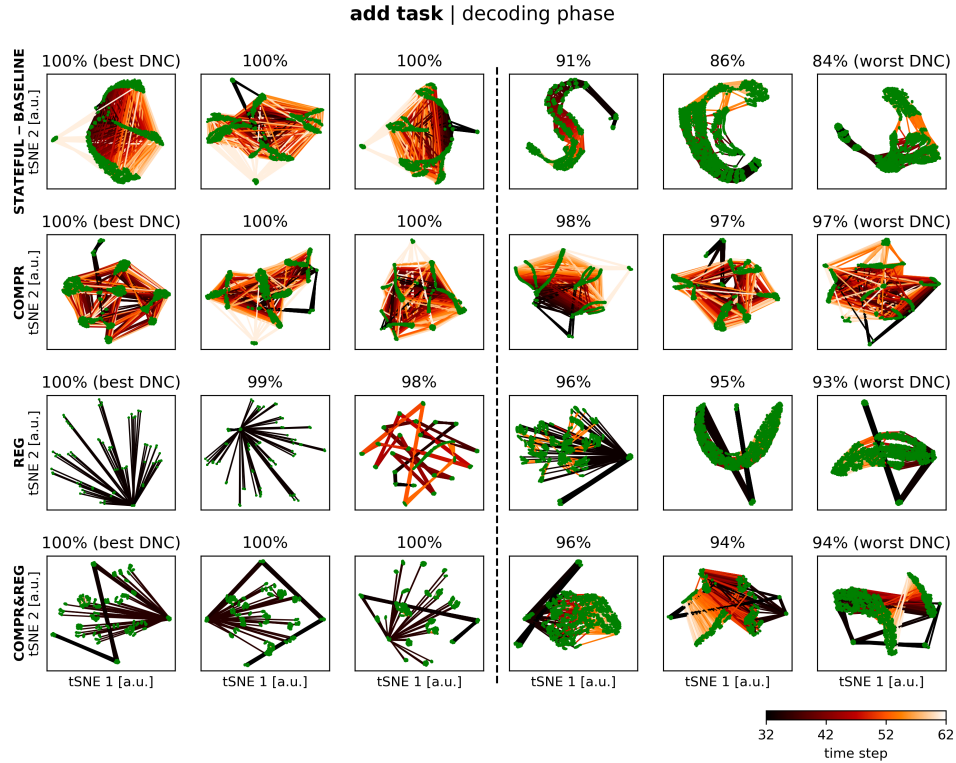


Fig. 17. Cell state trajectories from the decoding phase of the add task projected with t-SNE.

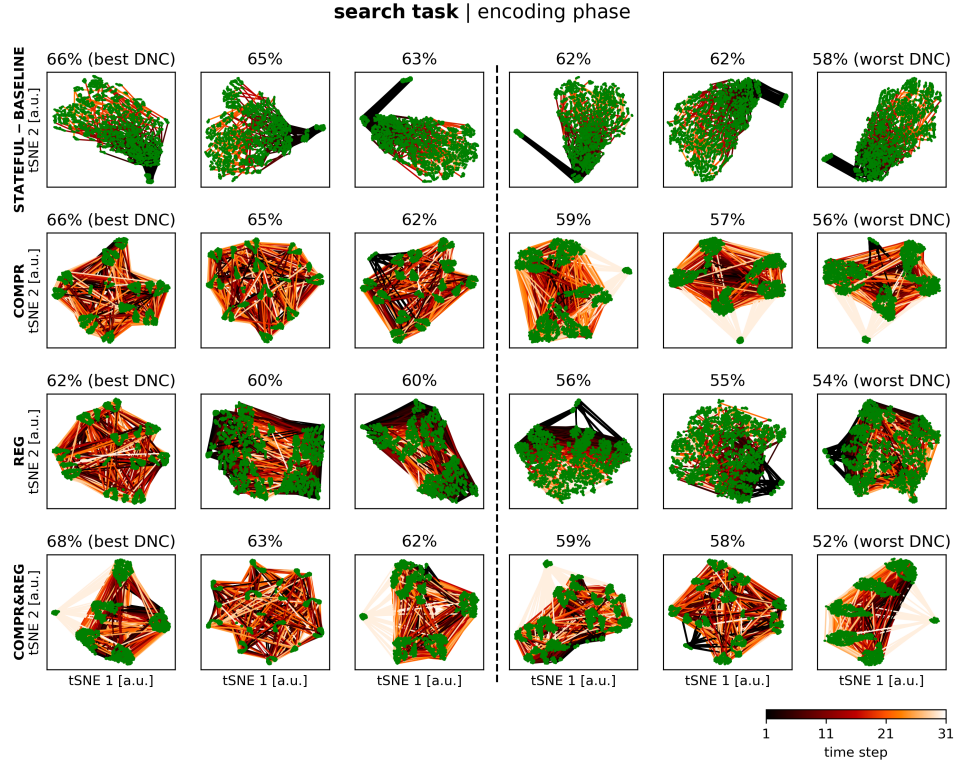


Fig. 18. Cell state trajectories from the encoding phase of the search task projected with t-SNE.

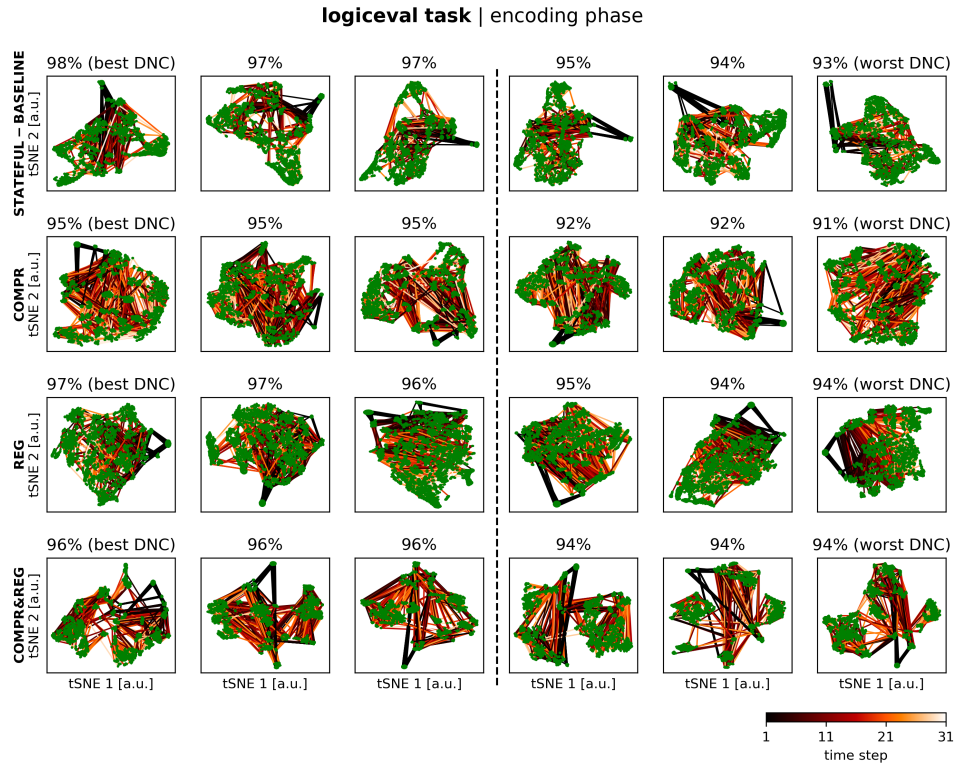


Fig. 19. Cell state trajectories from the encoding phase of the logic evaluation task projected with t-SNE.